Title
PRODUCTION OF K MESONS IN THREE-BODY STATES IN PROTON-PROTON INTERACTIONS AT 6 Bev/c

Author
Mandelkern, Mark Alan.

Publication Date
1967-11-01

UCRL-17943
c. 2

University of California

Ernest O. Lawrence Radiation Laboratory

PRODUCTION OF K MESONS IN THREE-BODY STATES IN PROTON-PROTON INTERACTIONS AT 6 BeV/c

Mark Alan Mandelkern
(Ph. D. Thesis)

November 1967

DISCLAIMER

UCRL-17943

UNIVERSITY OF CALIFORNIA

Lawrence Radiation Laboratory
Berkeley, California

AEC Contract No. W-7405-eng-48

PRODUCTION OF K MESONS IN THREE-BODY STATES IN PROTON-PROTON INTERACTIONS AT 6 BeV/c

Mark Alan Mandelkern
(Ph. D. Thesis)

November 1967

PRODUCTION OF K MESONS IN THREE-BODY STATES IN PROTON-PROTON INTERACTIONS AT 6 BeV/c

CONTENTS

UCRL-17943

PRODUCTION OF K MESONS IN THREE-BODY STATES IN PROTON-PROTON INTERACTIONS AT 6 BeV/c

Mark Alan Mandelkern

Lawrence Radiation Laboratory
University of California
Berkeley, California

ABSTRACT

An analysis is presented of data from an exposure of the LRL 72" liquid hydrogen bubble chamber to a 6 BeV/c proton beam. Processing of 9700 events, containing at least one observed neutral or charged decay has yielded 1748 examples of the reaction proton + proton → hyperon + K meson + nucleon. Production cross sections for these three body reactions are

$$\sigma(\Lambda K^+p) = 54\ ^{+3}_{-5}\ \mu b$$

$$\sigma(\Sigma^oK^+p) = 17\ ^{+4}_{-2}\ \mu b$$

$$\sigma(\Sigma^+K^op) = 26 \pm 4\ \mu b$$

$$\sigma(\Sigma^+K^+n) = 57 \pm 7\ \mu b$$

Strong N* production is observed in all channels. In particular one or more T=1/2 resonant states with mass near 1700 MeV/c^2, decaying into ΛK^+, and a T=3/2 resonance with mass 1920 MeV/c^2, decaying into ΣK, are produced. The final states ΛpK^+ and Σ^+K^+n are studied in detail. In both cases the data are consistent with a single pion exchange mechanism modified by a form factor and inconsistent with kaon exchange. The remaining two reactions are found qualitatively to have these properties as well.

as quasi-two-body reactions. For example, final states with three and four particles produced in K^+p interactions are dominated by K*(891) and N*(1236) production. At 2.7 GeV/c 88% of the $K^+p \rightarrow K^0p\pi^+$ channel proceeds with either K* or N* formation and 56% of the $K^0p\pi^+\pi^-$ events are produced as K*N*.[4] These results are typical.

Cross sections for these quasi-two-body reactions appear to possess quite well defined energy dependence, determined by the nature of the particle whose exchange seems to dominate the process. The equation $\sigma \sim P_{beam}^{-n}$ roughly fits all of these reactions and n is about 0.2, 1.5, 2.0, and 4.0 for "diffraction", non-strange meson exchange, strange meson exchange, and baryon exchange respectively.[5]

We have undertaken a study of proton interactions in the LRL 72" liquid hydrogen bubble chamber to search more intensively for baryon-baryon states and to investigate the general details of nucleon-nucleon reaction mechanisms, particularly resonance production via single particle exchange. We are concerned with the characteristics of hyperon production in three-body final states via the channels

$$pp \rightarrow \Lambda K^+p \quad .... \quad (a)$$
$$\Sigma^0K^+P \quad .... \quad (b)$$
$$\Sigma^+K^0p \quad .... \quad (c)$$
$$\Sigma^+K^+n \quad .... \quad (d)$$

The states produced in these reactions would appear to be most suitable for elucidation of final-state hyperon-nucleon interactions, whose effects might be obscured in states including pions by the presence of Y*, N*, and K* resonances. In addition, each of these reactions

permits comparison with the one-pion and one-kaon exchange models since hyperon-K associated production and K-nucleon scattering are fairly well studied processes.

The data reported result from analysis of approximately 500,000 photographs, taken in two separate running periods, of interactions of protons in a beam averaging ten particles per pulse. The incident momentum was 6.10 ± 0.02 BeV/c during the first running period and 6.00 ± 0.02 during the second. In Section II we discuss the experimental procedure, including the beam setup, scanning and measuring of the film, and subsequent data reduction. Section III contains a discussion of the determination of cross sections and Section IV is devoted to the search for dibaryon resonances and analyses of N* production in these reactions. In Section V we test the predictions of pion and K exchange modified by form factors. Reactions (b) and (c) provide too little data of sufficient quality for a meaningful analysis and are not considered in as much detail as reactions (a) and (d). Finally we test the prediction of exact SU_3 symmetry for three-body final states in pp reactions in Section VI.

II. EXPERIMENTAL PROCEDURE

Protons with momentum 6 BeV/c produced at 7° to the Bevatron External Beam in a target 3/8" high, 1/4" wide and 1/2" long were transported to the bubble chamber using the arrangement shown schematically in Fig. 1. The optical elements determining the focal properties of the beam at the uranium collimator were the first quadrupole pair, which yielded vertical magnification 0.5 and unit horizontal magnification, and two bending magnets producing a dispersion of about one inch per 1% $\Delta P/P$. Momentum definition of $\pm 0.15\%$ was provided by the slit, of dimensions 1/2" vertically and 1/4" horizontally, in the 12" thick uranium collimator; spatial acceptance was ~.01 millisteradians. To allow multiple operation of external beam foci, targeting techniques were needed which would minimize interference with external beam optics since the target could not conveniently be located at an image position of the Bevatron External Beam. In the first running period, during which about half the photographs were taken, a polyethylene target was fixed in position in the beam. During the remainder of the run a copper target was fixed at a distance of 3/4" from the normal external beam position and the beam deflected on to it by a magnet[6] pulsed on for approximately 500 μsec. In this way, intensity control independent of Bevatron intensity was achieved with the remainder of the beam available for other experiments. Beam intensity required was $\sim 10^{11}$ protons/pulse for the first targeting arrangement and $\sim 5 \times 10^{10}$ protons/pulse for the second for a flux of 30 protons. Increased efficiency of operation was achieved with dynamic intensity control provided by a pulsed parallel electromagnetic separator operated

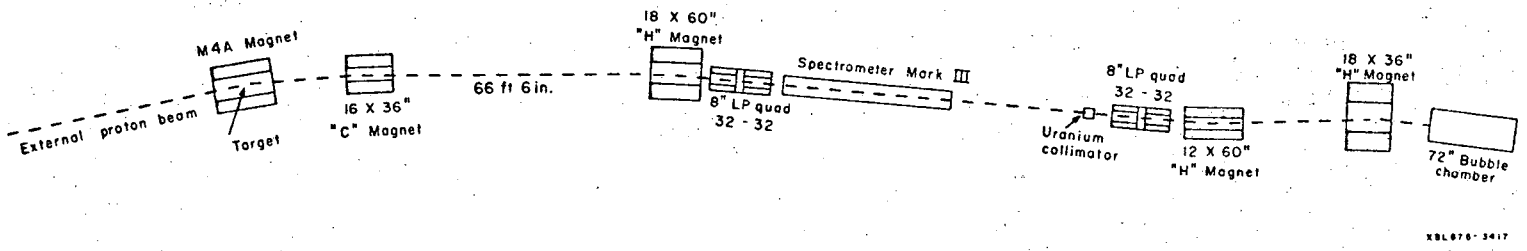

Fig. 1. Schematic of experimental arrangement.

with a 4" gap and 150 kilovolts between the plates.[7] An appropriate signal from a preset scalar reading the output of counters directly before the entrance window of the bubble chamber triggered a spark gap across the spectrometer plates which discharged them in 2 μsec. The magnetic field remained and caused the beam to be deflected 3/4" vertically, off slit S2 into the uranium collimator. In this way the usual variations in beam intensity due to statistical fluctuations and accelerator instability were largely eliminated. With a total beam in the channel of about 30 particles per pulse, the beam at the chamber was maintained constant to within two tracks per picture. Contamination from single pion production in the target was small since the primary proton beam and the secondary protons from the target were set to differ little in momentum, while the secondary pions had considerably lower momentum. A measurement made in a similar beam[8] using a Cerenkov counter to distinguish pions from protons indicated a pion contamination of less than 0.1%. This was neglected as a source of background events in the analysis.

The incident beam momentum was determined from measurements of non-interacting tracks and from well-identified examples of fits to elastic scattering. Both methods gave the same result, noted in Section I. The observed width of the beam momentum distribution was consistent with that expected only from measurement error, approximately 1%. However, we assign ± 0.5% uncertainty to the incident particle momentum for fitting purposes, allowing a rather larger spread than deduced from beam optics for effects such as scattering on slits and

windows.

B. Data Processing

The film was scanned for events of interest and three fourths of it was scanned a second time. All events containing one or more charged or neutral decays were recorded and measured with conventional digitized measuring machines. Geometrical reconstruction and kinematical fitting of events with neutral V's was done with the use of the program PACKAGE.[9] Of the three views measured, only the two chosen by the program to give maximum accuracy in determination of the dip angle of each track were used. Reconstruction and fitting of two-prongs with charged decays was done with TVGP-SQUAW[10] which uses measurements in three views for reconstruction.

A total of 7200 events of two-prongs and one neutral V, and 2500 of two prongs with the decay of either or both outgoing charged particles, candidates for events containing three final-state particles, were measured, the latter sample having been taken from only half of the film. A kinematic fit was attempted for every reaction hypothesis consistent with baryon number and strangeness conservation and involving at most one unobserved neutral particle. Identification of acceptable reaction hypotheses was established by the usual methods of requiring consistency of measured momenta with reaction kinematics and visually estimated bubble densities. The χ^2 for the kinematic fit was required to correspond to a probability level greater than 1% for reactions (a) and (c), and 5% for (b) and (d) because of greater contamination due to ambiguities. In addition, events were required to

be produced in a fiducial volume smaller than that specified for scanning, and containing 76% of the chamber volume.

Events with no acceptable fit were examined to determine whether they were consistent with the production of two missing neutrals, and 15% of the events with V's fall into this category. All others were remeasured but after two unsuccessful measurements were considered unmeasurable and not processed further. About 3% of the sample was unmeasurable. In this way 1302 events with neutral V's were identified as examples of three-body channels a, b, and c. Of these events, 45 were also consistent with four-body final states. They were assigned to the three-body category because the three-body fits are more constrained by the kinematical requirements. For reaction (b), $pp \rightarrow \Sigma^{o}pK^{+}$, one usually observes only the Λ from the Σ^{o} electromagnetic decay along with the charged prongs. The track bubble densities clearly do not distinguish between the Σ^{o} and Λ production hypotheses and a large fraction of the events are kinematically consistent with both. We resolve all the ambiguities between $\Sigma^{o}pK^{+}$ and ΛpK^{+} in favor of the Λ since the fit with a Λ has four constraints and that with a Σ^{o} only two. The decision in this case is greatly strengthened by appeal to the requirement that the angular distribution of any particle with respect to the incident beam direction be symmetrical about 90^{o} in the center-of-mass system. In Fig. 2 we show the angular distribution of the proton produced with a hyperon and K^{+} for the weighted total of 533 events with uniquely identified Λ's, together with that including the 504 events with ambiguous identification of the hyperon. Clearly the

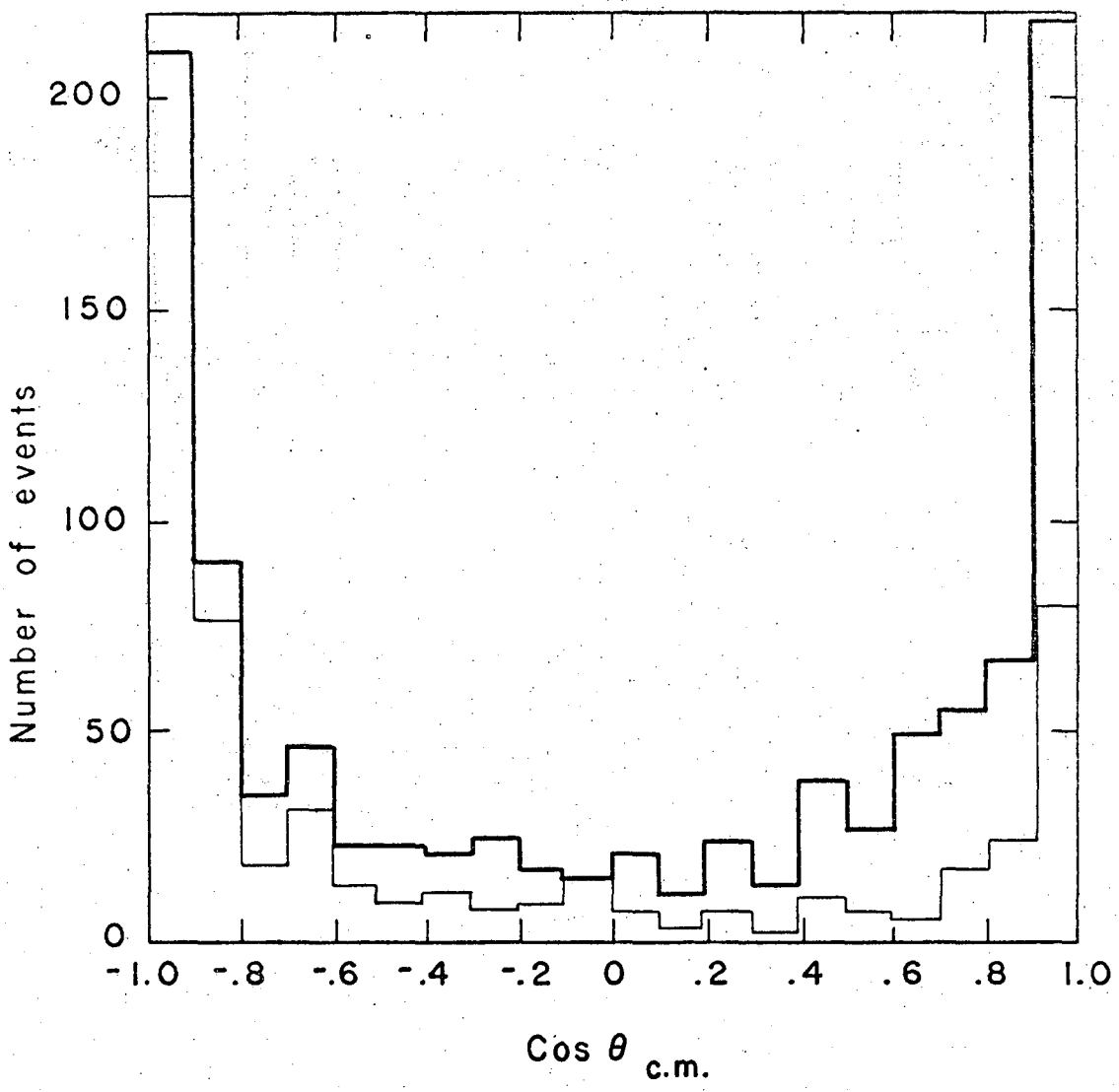

XBL676-3405

Fig. 2. Distributions of the cosine of the angle the final state proton makes with the beam proton in the overall center of mass, light line: only unambiguously identified examples of the reaction $pp \rightarrow \Lambda pK^+$, heavy line: total sample of ΛpK^+, including events ambiguous between hypothesis $pp \rightarrow \Lambda pK^+$ and $pp \rightarrow \Sigma^o pK^+$.

symmetry is improved if the events are combined. Thus, in all such cases of ambiguity the hyperon is considered to be a Λ. The angular distribution of the protons produced in unambiguous examples of the $\Sigma^{o}pK^{+}$ final state is shown in Fig. 3. This distribution is not nearly as symmetric as that for ΛpK^{+}, reflecting the greater difficulty in resolving ambiguities with the two constraint fit. The asymmetry is, however, in the same direction as that of the ambiguities which were assigned to ΛpK^{+} and thus does not result from inclusion of misidentified Λ production events. We conclude that the source of this asymmetry is ambiguity with four-body hypotheses which have one constraint, and that the four-body background plus events lost due to misidentification amounts to about 10% of the sample, judging from the number of ambiguous events and the size of the production asymmetry. We show in Fig. 4 distributions in the cosine of the rest frame decay angle of the Σ^{o}; Fig. 4a with respect to the normal to the plane containing the Σ^{o} and an incident proton in the $\Sigma^{o}K^{+}$ rest frame, and Fig. 4b with respect to the Σ^{o} direction. Both are quite consistent with uniformity. Since the decay $\frac{1}{2}^{+} \rightarrow \frac{1}{2}^{+} + \gamma$ is constrained to be isotropic the data is consistent with a relatively uncomtaminated Σ^{o} sample. We find that the distributions in these variables for events ambiguous with the ΛpK^{+} hypothesis show strong non-uniformity.

Since the reaction (d) always yields an unobserved neutral product, kinematical constraints may be applied only if the Σ^{+} momentum is known from measurement of the Σ^{+} track and/or measurement of the decay product track. In either event, the momentum is generally poorly

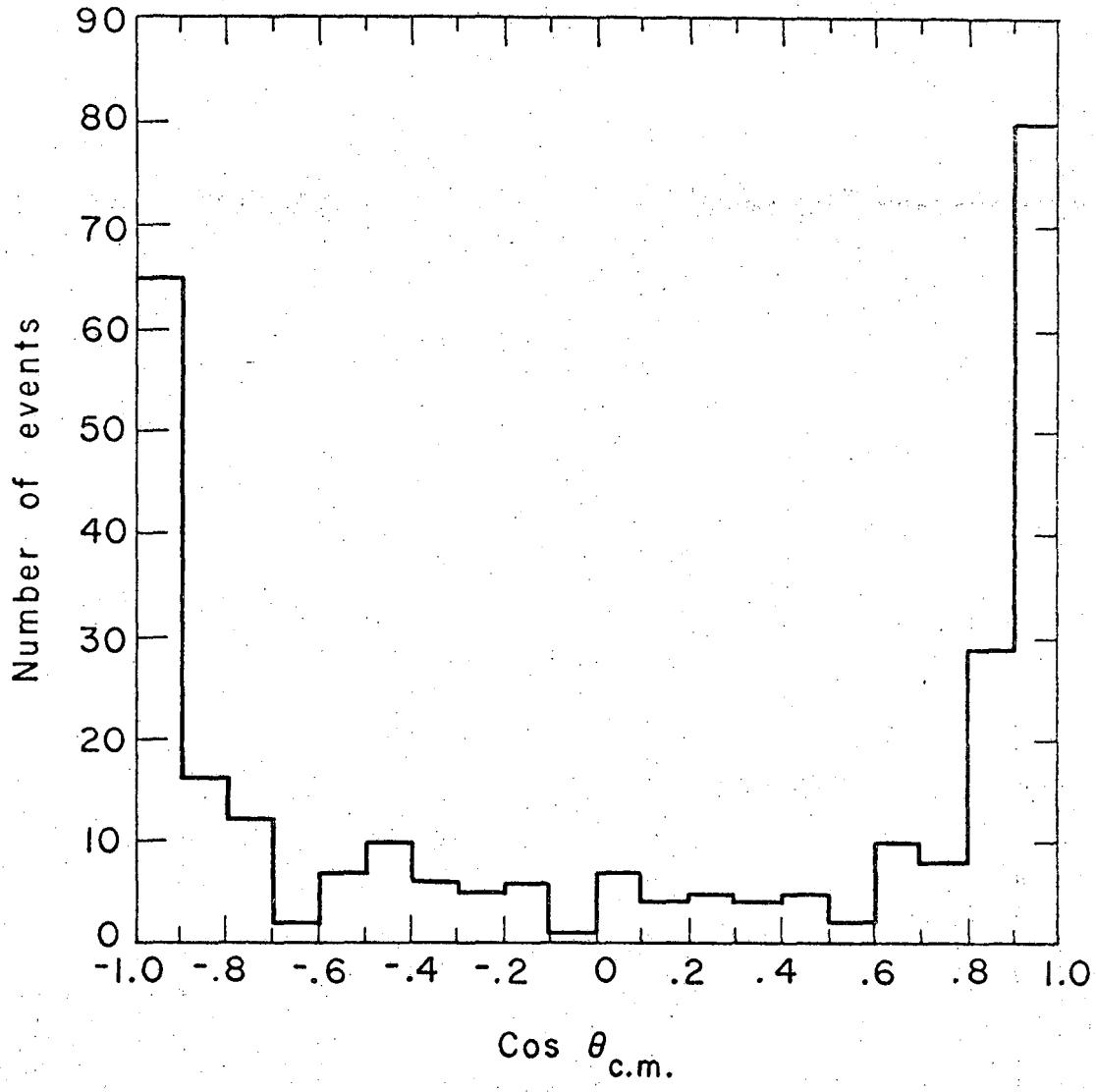

XBL 676-3406

Fig. 3. Distribution of the cosine of the outgoing proton center of mass angle for unambiguously identified examples of the reaction $pp \rightarrow \Sigma^{o} pK^{+}$.

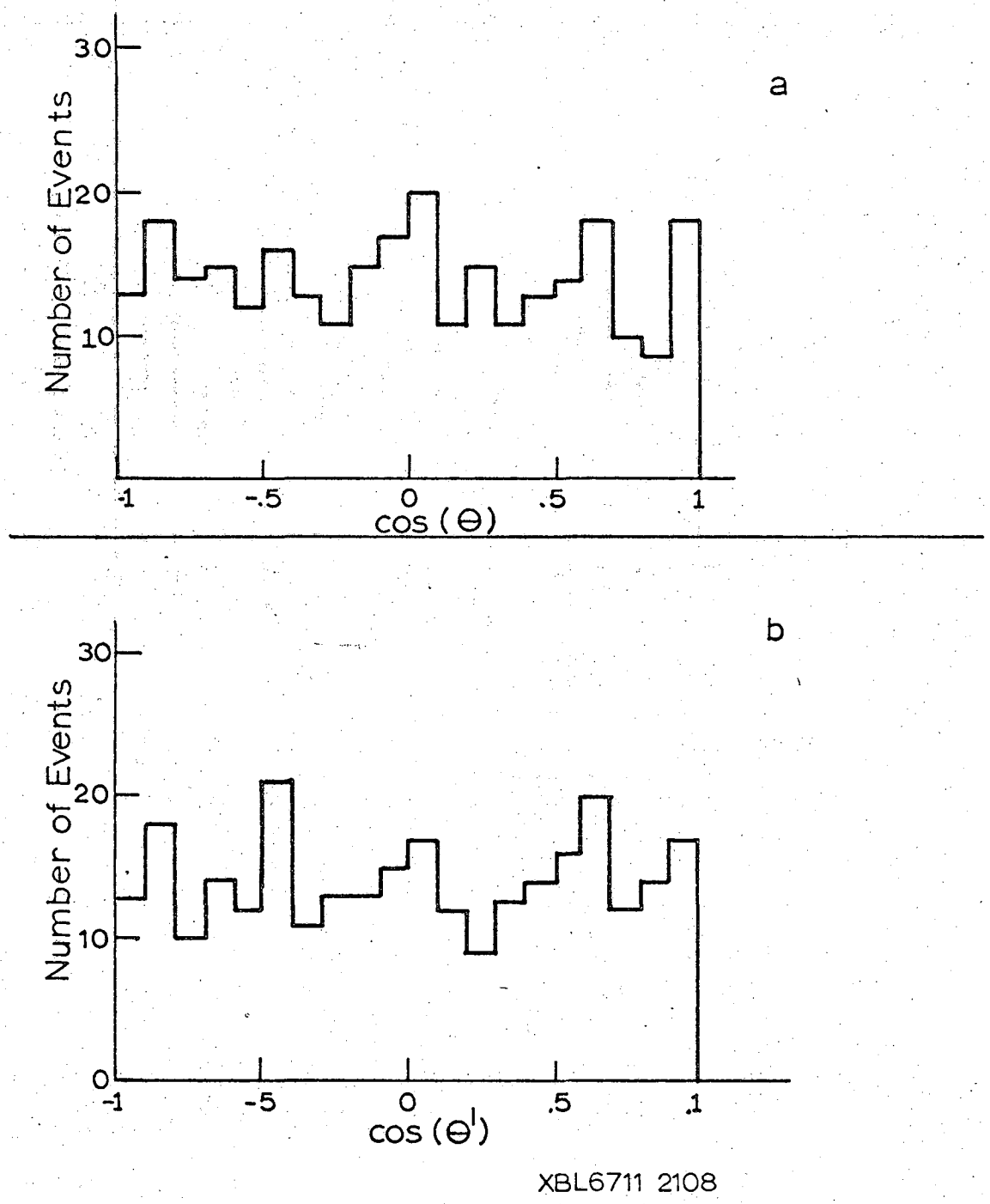

Fig. 4. Decay angular distributions of the Σ^o for the channel $\Sigma^o pK^+$; (a) θ is the angle between the Λ in the Σ^o rest frame and the Σ^o production plane normal. (b) θ' is the angle between the Λ and the Σ^o direction.

determined and kinematical ambiguities are more serious. Three kinds of ambiguities were present: those involved in (i) distinguishing between Σ^+ decays and K^+ decays, (ii) distinguishing $\Sigma^+ pK^o$ with unobserved K^o decay, and (iii) separating events with an additional, unobserved neutral. In fact only an insignificant number of the first and second kinds appear, fitting to the decay kinematics and bubble density estimates generally being sufficient to distinguish among the various hypotheses. Further, the ratio of observed numbers of $\Sigma^+ pK^o$ with K^o decay to the number with unobserved K^o decay, after correction for detection inefficiency and scanning biases, is 0.3 ± 0.1, indicating that the correct number of identifications of $\Sigma^+ pK^o$ events has been made. In the analysis of reaction (d) only the events consistent with $\Sigma^+ \rightarrow n\pi^+$ were used. This procedure is required since, to correct for scanning inefficiency, we impose a minimum projected decay angle cut-off of 10^o. The decay angle of the proton from a Σ^+ with momentum greater than 1.4 BeV/c is necessarily smaller than 10^o. We find that the corrected sample of data for reaction (d) is consistent with symmetry in the total center-of-mass frame and estimate from the number of ambiguities that contamination is $5 \pm 2\%$.

In these ways, ambiguities in identification were settled and events were assigned to particular categories. Table I gives the total number of observed events for each of the four reactions.

For each of the reactions we require that at least one strange particle decay is observed within the chamber fiducial volume. Events in which the decay occurs beyond this volume are obviously not found. In addition, a fraction of events occurring in the chamber escape detection in both scans. Corrections to the observed body of data, in addition

Table I. Event totals and cross sections for pp three-body reaction containing a K-meson at 6 BeV/c.

Channel	Observed number	Number satisfying kinematic criteria	Corrected number (c)	Cross section (μb)
ΛpK^+	916	813	1037	$54.2\ ^{+3}_{-5}$
$\Sigma^o pK^+$	254	227	285	$17.0\ ^{+4}_{-2}$
$\Sigma^+ pK^o$				26.0 ± 4
$\Sigma^+ \rightarrow \pi^+(n)$	87	109	131(b)	
$\Sigma^+ \rightarrow p(\pi^o)$	45		65(b)	
$\Sigma^+ p(K^o)$(a)				29 ± 5
$\Sigma^+ \rightarrow \pi^+(n)$	84		126	
$\Sigma^+ \rightarrow p(\pi^o)$	33			
$\Sigma^+ K^+(n)$(a)				57 ± 7
$\Sigma^+ \rightarrow \pi^+(n)$	255	148	395	
$\Sigma^+ \rightarrow p(\pi^o)$	72			

(a) Only half of the film was analyzed for the two prong with decay topology.

(b) This number does not contain a correction for small angle Σ^+ decays.

(c) Only cross sections contain corrections for unobserved decay modes.

to that due to ordinary scanning inefficiency, must then be made for inefficient detection of decays occurring with small laboratory angles or at very small or large distances from the production origin, as well as for undetected decays into neutral particles. Examination of the observed distributions in lifetime and in decay angle of unstable particles permits estimates to be made of the detection efficiency. In addition, the requirement of a symmetric production angular distribution aids in determining detection biases. To correct for these inefficiencies, each event was weighted by the inverse of the probability for detection within a specified kinematic region. This region is determined by requiring events to be within a fiducial volume, to have decays with projected opening angles greater than 10° and less than 75° and lengths greater than minima determined by particle identification: 1.5 cm for Λ's and K^{o}'s, 1.0 cm for Σ^{+}'s. These corrections are discussed in Appendix A. Their magnitudes may be inferred from the corrected numbers of events listed in Table I. The correction factors for unobserved decay modes are a) 2.9 for K^{o}'s, since only $K_1 \rightarrow \pi^{+}\pi^{-}$ events are observed, b) 2 for Σ^{+}, since we do not use $\Sigma^{+} \rightarrow p\pi^{o}$ decays, and c) 1.5 for Λ's, for only $\Lambda \rightarrow p\pi^{-}$ decays are observable. Here we use branching ratios from Ref. 11.

III. PRODUCTION CROSS SECTIONS

Reaction cross sections were determined from the number of events, suitably corrected, in a channel, and the incident proton flux as determined by a count of beam tracks in frames selected at regular intervals throughout the film.

We have

$$\sigma_i = \frac{\text{Corrected number of interactions in channel } i}{\text{No. of incident particles} \times \text{No. of scattering centers/unit area}}$$

$$= \frac{N_i}{DL}$$

where D is the density of protons in the chamber and L is the total beam track length available. N_i is given by

$$N_i = \sum_j w_j/\epsilon_i,$$

the weighted total of events divided by the scanning efficiency for channel i.

i) We determined L by counting beam tracks in every 50th frame throughout the film. Only those tracks traversing the scanning fiducial volume without interacting were counted and the average number of tracks/frame is $N_E = 10.2 \pm 0.2$. The error reflects the reproducibility of this number rather than statistical error. Since the total p-p cross section is 40.6 ± 0.1 at this energy[12] the beam is severely attenuated as it passes through the chamber. That is, if N_B protons enter at y = 0,

$$N(y) = N_B e^{-D\sigma_T y}$$

have not yet interacted at y. Then the track length available to a single channel in length ℓ is

$$L = N_E e^{D\sigma_T \ell} \int_0^{\ell} e^{-D\sigma_T y} dy .$$

Since elastic scatters with momentum transfer < 0.01 are essentially unobservable because of the slow recoil proton (< 100 MeV/c corresponding to a 3 mm track length), we use σ_T = 39 mb, correcting with the differential cross sections of Reference 13.

D, the hydrogen density, has been determined for standard running conditions of the 72" chamber to be 0.060 ± 0.001 from measurements of the length of muons from stopping positive pions. The hydrogen temperature measured during our exposure was 27.5 ± 0.2° K which gives a value for D consistent with the above. This value corresponds to $(0.060 \pm 0.006) \times 10^{23}$ protons/cm^3. With a fiducial volume length ℓ = 145 cm and 569,718 frames we find

$$L = (9.88 \pm 0.3) \times 10^5 \text{ cm}.$$

ii) The scanning-measuring efficiencies were deduced from a comparison of processed events from the two scans. If the number of events found and successfully processed in both scans is N_{AB}, and the numbers found and processed only in each of the two scans are N_A and N_B respectively, the scanning-processing efficiencies are

$$\epsilon_A = N_{AB}/(N_B + N_{AB}) \text{ and } \epsilon_B = N_{AB}/(N_A + N_{AB})$$

respectively.[14] We find ϵ_A = 0.80 ± 0.03 and ϵ_B = 0.81 ± 0.03 for our two scans for both the two prong with neutral V and two prong with

charged decay event types.

We quote cross sections in Table I. Errors contain statistical errors which are given by the application of Poisson statistics to a weighted collection of events, thus if

$$N_i = \sum_j w_j, \quad (\delta N)^2 = \sum_j w_j^2 .$$

We include as well an estimated error ±5% resulting from misidentifications and uncertainties in the magnitudes in the various corrections.

IV. ANALYSIS OF FINAL STATE INTERACTIONS

A. General Features

The four states studied, ΛpK^+, $\Sigma^o pK^+$, $\Sigma^+ pK^o$, and $\Sigma^+ K^+ n$ have similar properties in many respects. We will discuss them simultaneously as much as possible. Figures 5, 6, 7 and 8 are scatter plots of the squares of the effective masses of hyperon-nucleon vs hyperon-kaon systems. In each case a non-uniform density within the kinematic boundary of the Dalitz plot is apparent. A strong concentration of data points is noted at low values of Y-K mass, particularly in the ΛK^+ and $\Sigma^+ K^+$ systems. In no case is there a clearly defined region in hyperon-nucleon effective mass within which the density of points is strikingly larger than in others. Rather, only in a region defined by limits on YK^+ effective mass is there such a concentration. The existence of only ΛK^+ and ΣK final-state interaction is demonstrated more conclusively in the effective mass distributions of Figs. 9, 10, 11, and 12 shown together with the corresponding phase space distributions. Corrections to the data have been made here for observational biases, so that each observed event is weighted as discussed above. The bin heights in each histogram are the sums of the weights for individual events falling into the relevant bins, with statistical errors computed as discussed in Section III.

The weights for reactions (a), (b), and (c) are relatively constant with average values 1.3, 1.3 and 1.8 respectively. The weights for reaction (d) are distributed over a broad range with average value 2.6; consequently, error bars are displayed on the histograms of Figs. 12 and 21b. In fact, none of the conclusions are substantially altered when unweighted

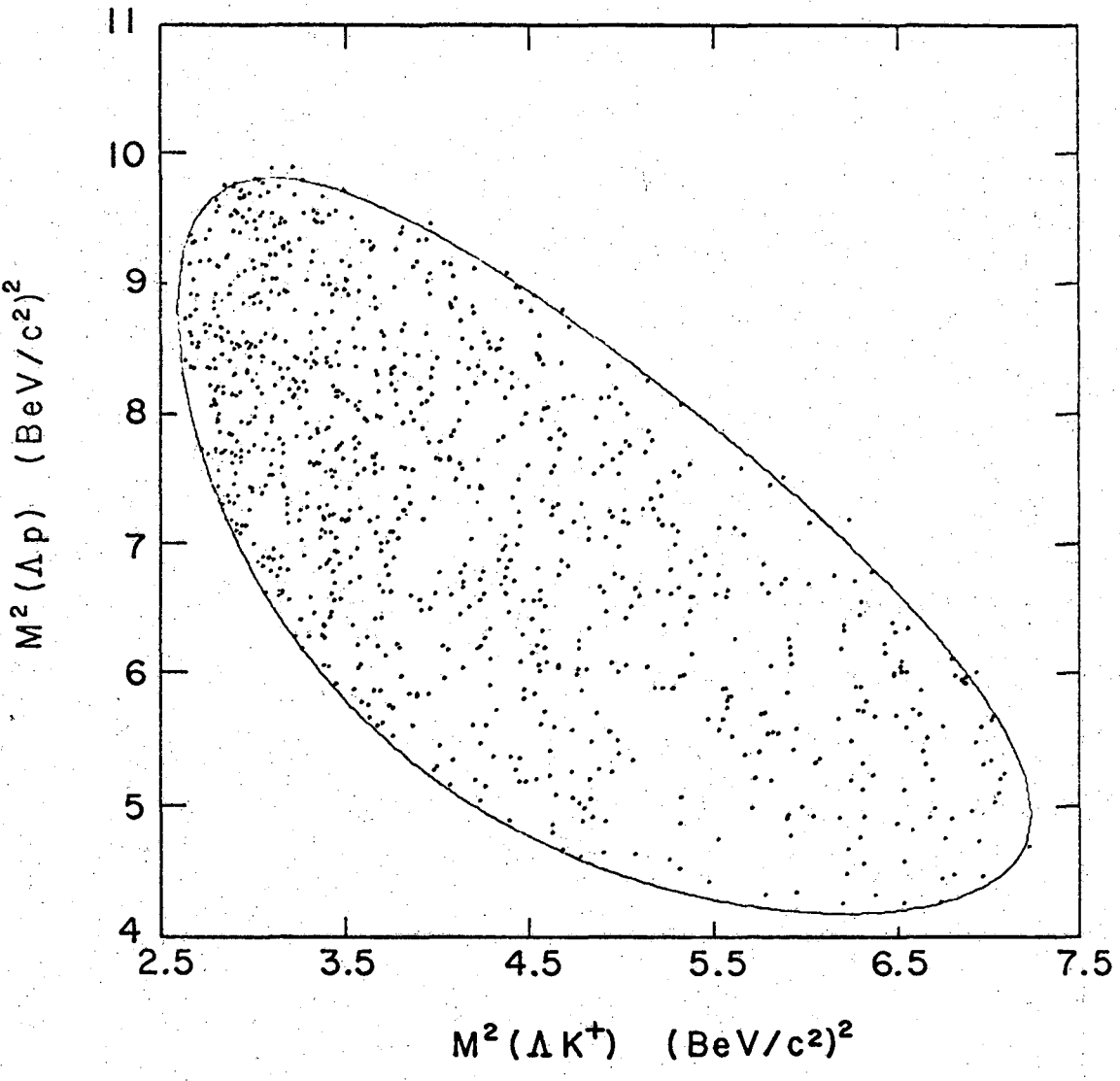

Fig. 5. Dalitz plot for reaction $pp \rightarrow \Lambda pK^{+}$.

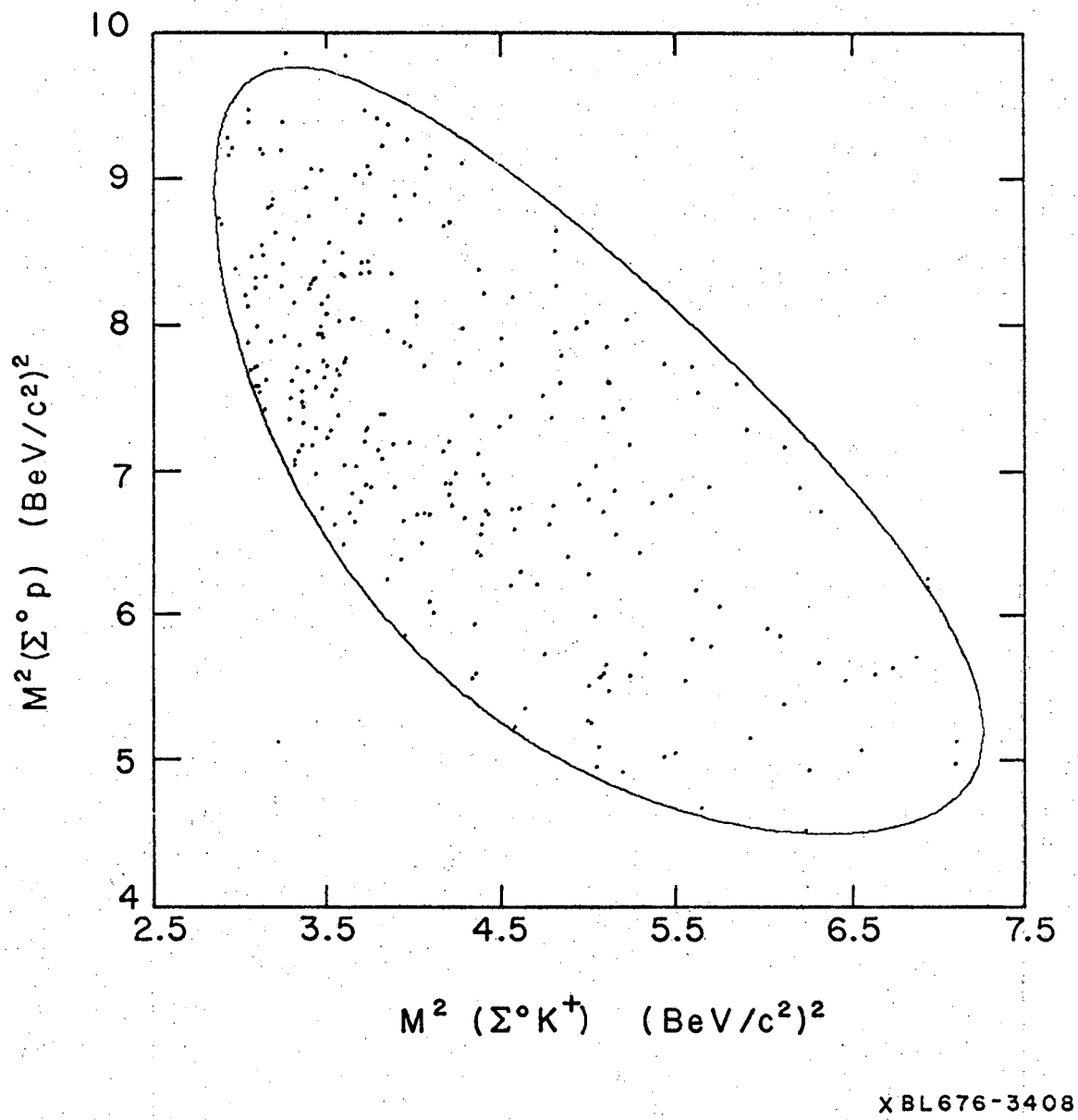

Fig. 6. Dalitz plot for reaction $pp \rightarrow \Sigma^{o}pK^{+}$.

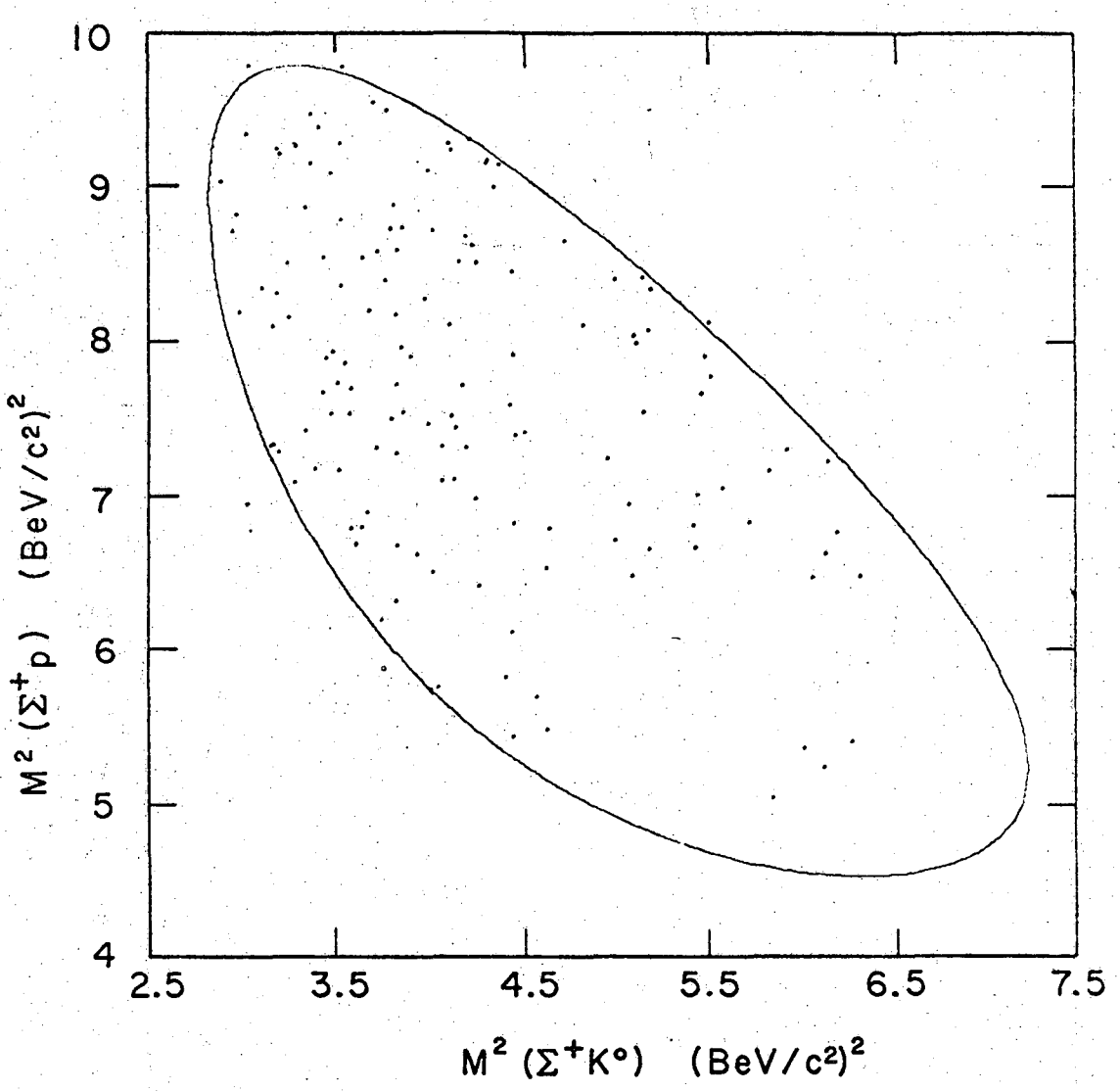

Fig. 7. Dalitz plot for reaction $pp \rightarrow \Sigma^+ pK^o$.

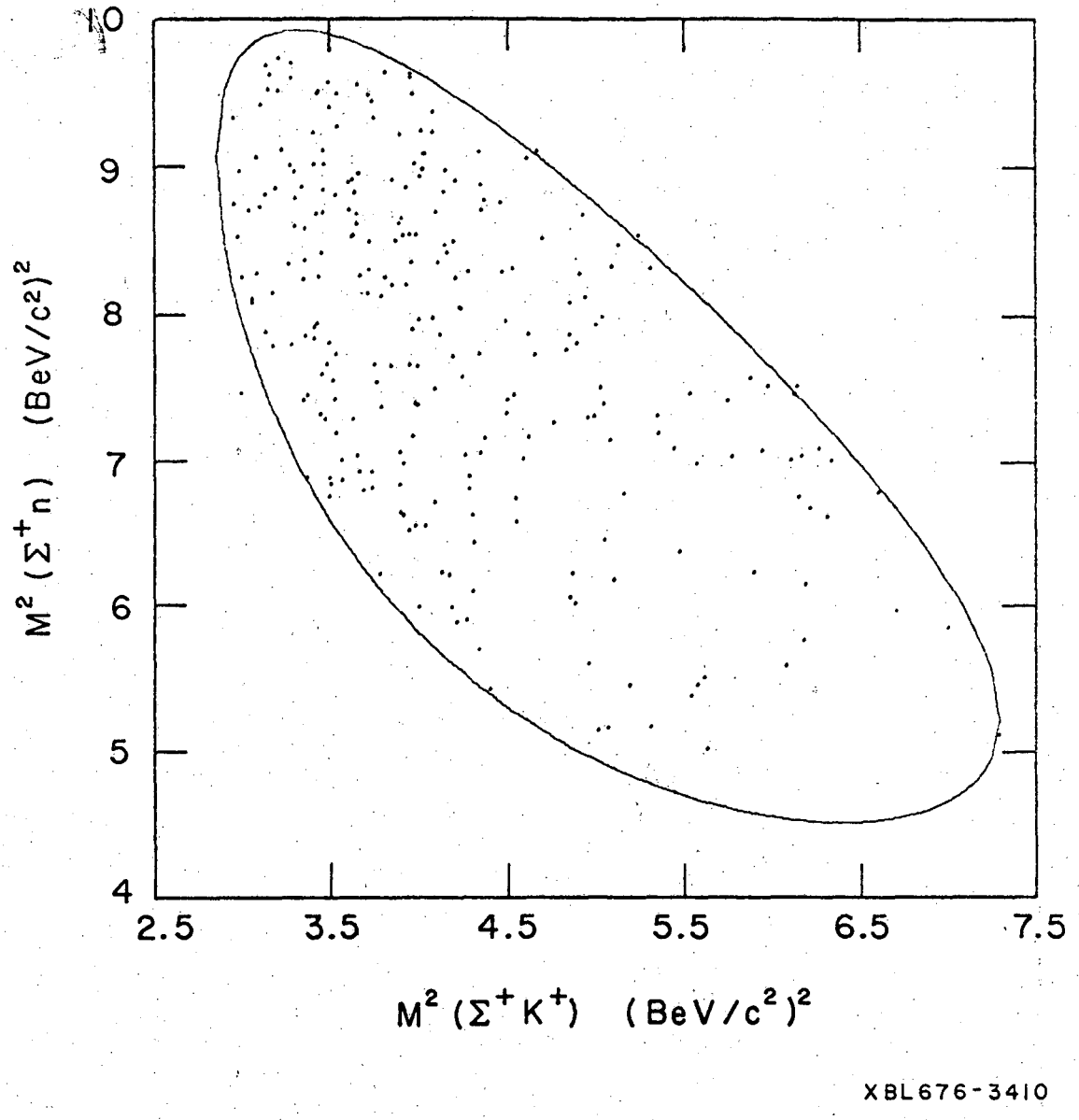

Fig. 8. Dalitz plot for reaction $pp \rightarrow \Sigma^+ nK^+$.

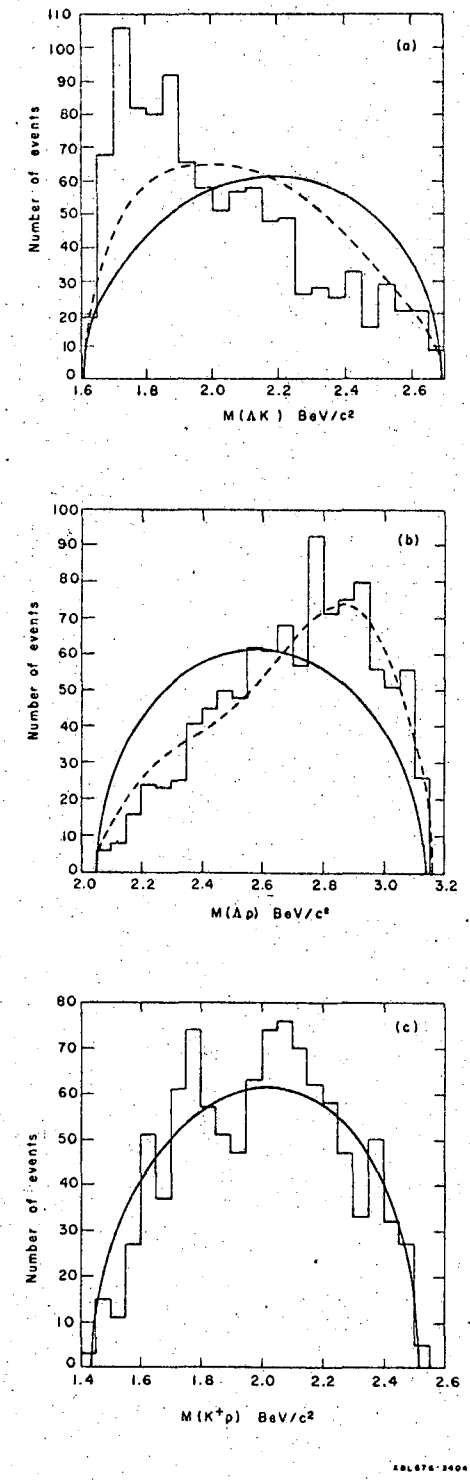

Fig. 9. Mass distributions in the channel ΛpK^+; (a) $M(\Lambda K^+)$, (b) $M(\Lambda p)$, (c) $M(K^+p)$. The solid curves are phase space distributions while the dashed curves represent the effect of reflections, as discussed in the text.

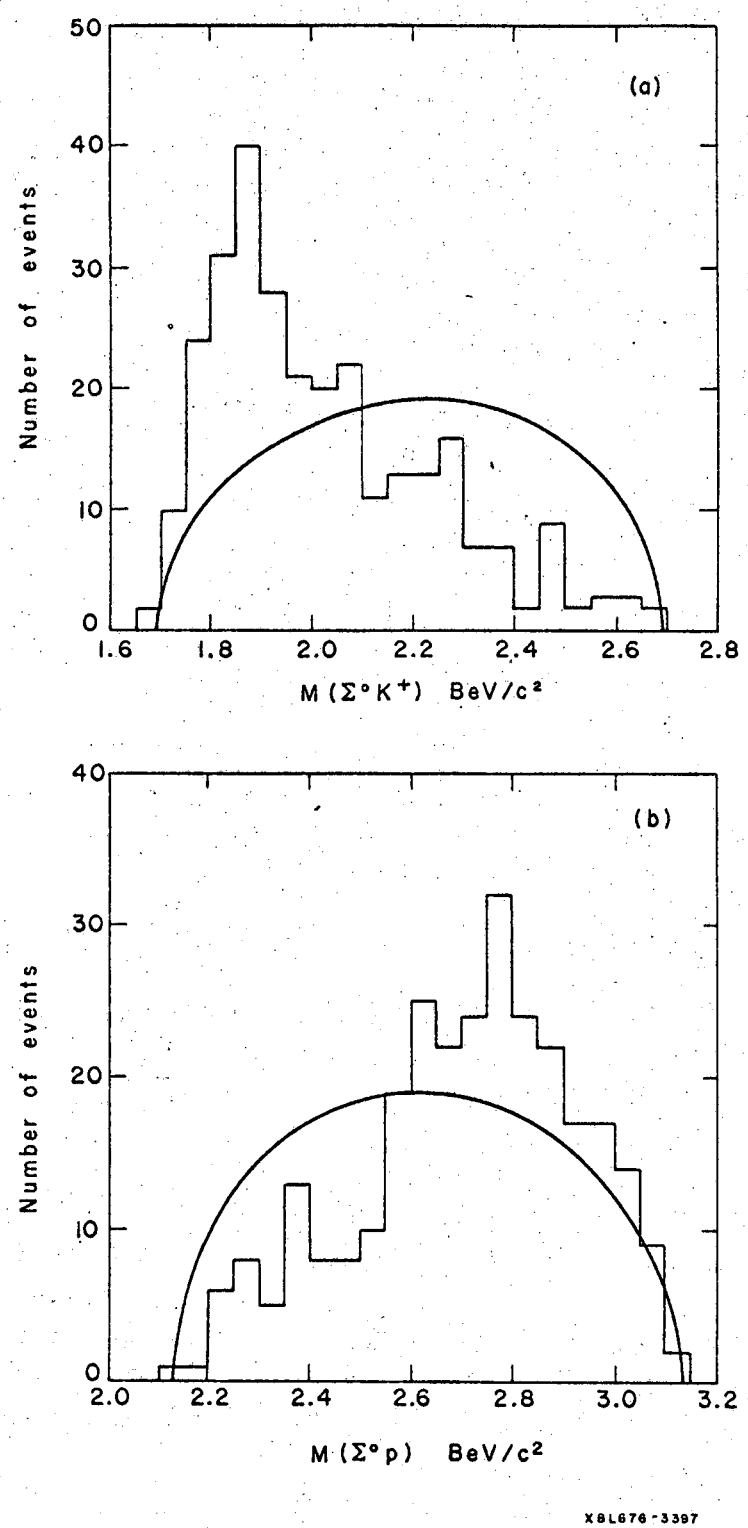

Fig. 10. Mass distributions in the channel $\Sigma^{o}pK^{+}$; (a) $M(\Sigma^{o}K^{+})$, (b) $M(\Sigma^{o}p)$. The curves are phase space distributions.

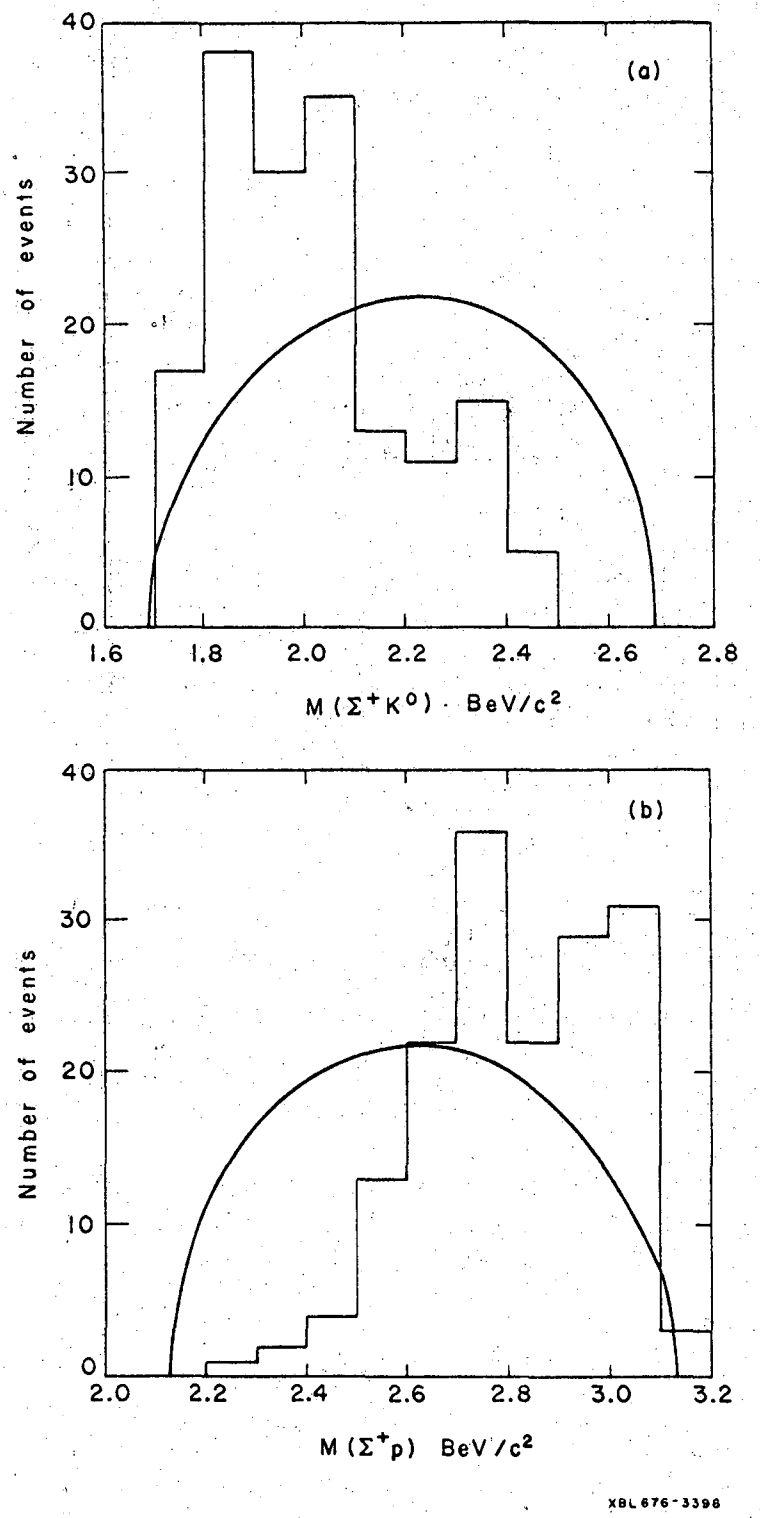

Fig. 11. Mass distributions in the channel $\Sigma^+ pK^o$; (a) $M(\Sigma^+K^o)$, (b) $M(\Sigma^+P)$. The curves are phase space distributions.

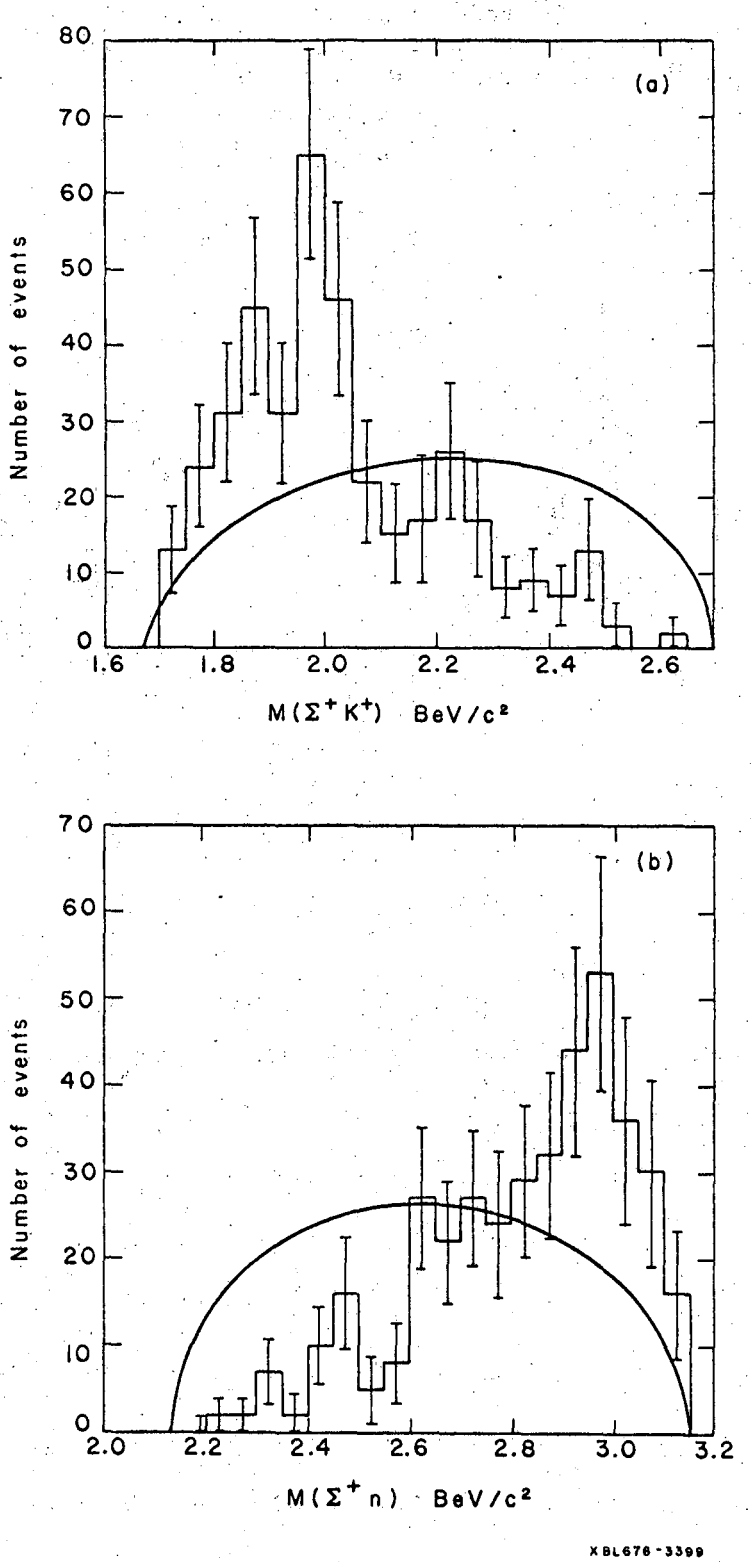

Fig. 12. Mass distributions in the channel Σ^+nK^+; (a) $M(\Sigma^+K^+)$, (b) $M(\Sigma^+P)$. The curves are phase space distributions.

distributions are considered. This is the case because only about 10% of the events with visible decays of neutral V's and 30% of the number with charged decays, are actually missing from the sample. In addition, the detection inefficiencies are not strongly dependent on the momentum and angular distributions.

All the Y-N and Y-K mass distributions show considerable deviations from the statistical distribution, but most of the further discussion will be limited to the ΛpK^+ and $\Sigma^+ nK^+$ states for a number of reasons. In the first state the hyperon-kaon system occurs only with isotopic spin $T = 1/2$ and in the latter only with $T = 3/2$, so that the analysis of resonance production is simplified. The $\Sigma^o pK^+$ and $\Sigma^+ pK^o$ reactions appear qualitatively to have properties similar to those discussed below and the samples of these are severely limited statistically and probably more contaminated. Analysis of the latter reactions does not add to the conclusions about final-state interactions nor to the further elucidation of the production dynamics.

We have noted the non-uniformity in the Dalitz plot and the corresponding enhancements at low hyperon-kaon mass and high hyperon-nucleon mass. While it is not possible, in general, to demonstrate rigorously which of the two-body combinations are in resonance, we can nevertheless argue persuasively that the details of the non-uniformity are consistent with the production of only Y-K resonances. A simple check of this hypothesis consists of alternately assuming production of the Y-K and Y-N systems with the observed mass distributions, followed by isotropic decay in their center-of-mass frames, and calculating the

expected reflections in the Y-N and Y-K systems, respectively. The results of such calculations are shown in Fig. 9 for the ΛpK^+ reaction. It is clear that the Λp peak can be understood as a reflection of a ΛK^+ enhancement, while the converse does not hold.

The above assumption of an isotropic disintegration of the two-body system cannot be completely justified. The break-up angular distributions of either two-body system can be readily obtained from the Dalitz plots, Figs. 5-8. The ordinate and abscissa may be interpreted respectively as the square of the Y-nucleon mass and the cosine of the angle between the hyperon and the K line of flight in the Y-N center-of-mass system. The latter angle need not be isotropically distributed, as a consequence of the production mechanism, or final-state interactions. A new hyperon-nucleon resonance with a pathologically anisotropic decay distribution could be invoked to explain the overall distribution in the Dalitz plot and the Y-K enhancement as a reflection. It is quite unnecessary to invoke such a new resonance with complicated properties, but we rather attribute the distribution purely to already well-established Y-K resonant interactions, specifically $N^*_{1/2}(1688)$ and $N^*_{3/2}(1920)$.

This conclusion is greatly reinforced by the observation that the Y-K production is predominantly peripheral and consistent with a single pion exchange model as discussed below. It should be noted that if those events produced with low momentum transfer to the initial proton are eliminated from the Λp mass distribution, a spectrum results that is in excellent agreement with phase space, as seen in Fig. 13. Thus

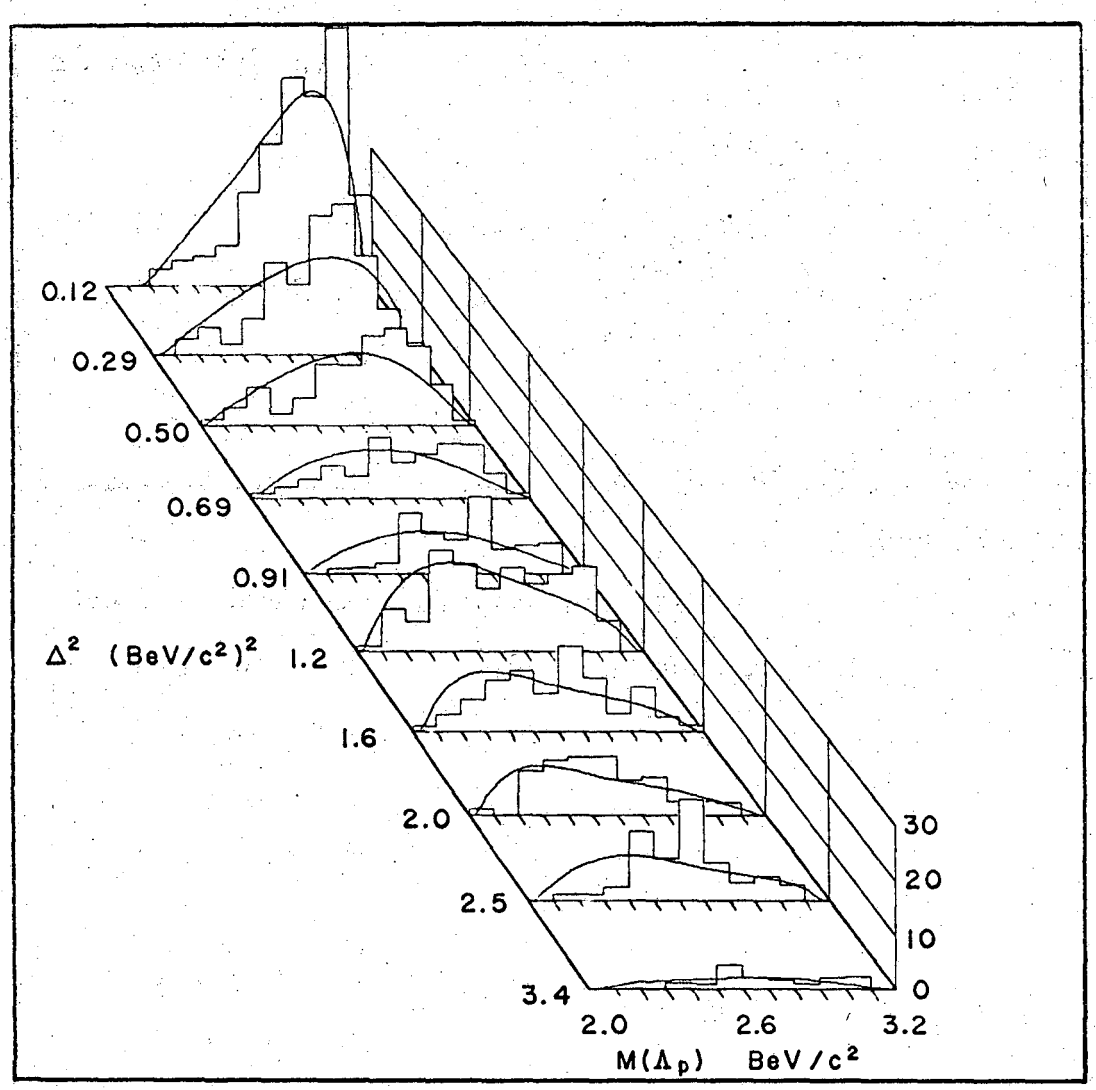

XBL676-3413

Fig. 13. The Λ-p mass distribution for the channel ΛpK^+ shown as a function of momentum transfer to the proton. The curves are phase space distributions.

even in the region where peripheralism does not dominate, there is no suggestion of a dibaryon resonance. In calculating momentum transfer, there are, of course, two values for each event since the initial state protons are indistinguishable. We use the smaller momentum transfer to define the identities of the initial state protons when comparing with dynamical models and require our theoretical calculations to be consistent with this procedure. Such a choice is suggested by the strong peaks at low momentum transfer, which characterize peripheral production. This procedure is well justified by the further demonstration below that the mechanism is indeed peripheral.

The Λp and ΛK^+ mass spectra may be understood to result, in part, from a quasi-two-body process, $pp \rightarrow N^*_{1/2}p$, proceeding via a peripheral mechanism, with subsequent decay of the N^* into ΛK^+. The conclusion that there is no evidence for a Λp resonant state is in agreement with that of Bierman, et al.[15] The K^+p mass distribution for this reaction, Fig. 9c, shows structure not observed in K^+p elastic scattering with enhancements at 1.8 and 2.1 BeV/c^2. These features cannot be simply explained as reflections of the $N^*_{1/2}(1688)$ production. However, their absence in K^+p elastic scattering suggests that the peaks observed here are not resonances, but rather kinematical effects associated with the full description of the production process, or statistical fluctuations.

Consequently we conclude that we have observed no dibaryon resonances in either the T=1/2 or the T=3/2 state in the mass range from 2.05 to 3.14 BeV/c^2. It is conceivable that a dibaryon resonance in this range would be difficult to detect above the

background of peripherally produced events in this reaction. Nevertheless the absence of distinct localized enhancements in the hyperon-nucleon mass spectrum leads to the above conclusion. Further, we estimate that the cross section for the production of the enhancement reported by Melissinos et al.[3] is less than 0.2 μb in the present experiment.

B. Nucleon Isobar Production

Analyses of pion nucleon elastic scattering have revealed evidence for the existence of three T = 1/2 resonances near 1690 MeV and one T = 3/2 resonance near 1920 MeV total c.m. energy.[11] The properties of these resonances inferred from the phase shift analyses are listed in Table II. We interpret the observed resonance production as production of these pi-nucleon resonances and their subsequent decay into hyperon and kaon.

Analysis of the angular and polarization distributions observed in $\pi^+ p \rightarrow \Sigma^+ K^+$[16] show that this reaction proceeds in part through an $F_{7/2}$ resonance at 1925 MeV with width Γ = 175 MeV, consistent with the parameters of the resonance observed in pi-nucleon elastic scattering. The partial width of the $F_{7/2}$ into $\Sigma^+ K^+$ was found to be about 1 MeV. Our peak in the $\Sigma^+ K^+$ mass spectrum in the channel $\Sigma^+ n K^+$ is naturally interpreted as due to the production of this resonance and its subsequent decay into $\Sigma^+ K^+$. To estimate the rate of resonance production, the distribution in Δ^2, momentum transfer to the neutron, and M, $\Sigma^+ K^+$ effective mass, was fitted to the expression

Table II. Pion-nucleon resonances between 1600 and 2000 MeV/c^2.[a]

N*	Resonant State	M^o(MeV)	$\Gamma_{elastic}$ (MeV)	$\Gamma_{inelastic}$ (MeV)
T=3/2	$F_{7/2}$	1920	100	100
T=1/2	$S_{1/2}$	1700	240	0
	$D_{5/2}$	1670	56	84
	$F_{5/2}$	1688	72	38

(a) Values are quoted from Reference 11.

$$d^2\sigma = \frac{1}{(\alpha+\Delta^2)^2}\left[\frac{q}{M}\ 1 + c\,\frac{\Gamma_{\Sigma^+K^+}(M)}{(M_o^2-M^2)^2 + M_o^2\,\Gamma^2}\,\frac{M^2}{q}\right] dM^2 d\Delta^2 \qquad (1)$$

which is an incoherent sum of resonance and background. The form factor $1/(\alpha+\Delta^2)^2$ is used to parameterize the strong peripheralism shown in the data. Here q is the momentum of the Σ^+ in the Σ^+K^+ rest frame, M_o the resonance energy quoted in Table II, Γ the total width and c a number which characterizes the production cross section. The energy dependent partial width into the channel $\Sigma^+ + K^+$ was taken to be

$$\Gamma_{\Sigma+K^+} = \Gamma^o_{\Sigma+K^+}\,\frac{(q/q_o)^{2\ell+1}(M_o/M)}{(q^2+X^2)^\ell/(q_o^2+X^2)^\ell} \quad . \qquad (2)$$

The "partial width" $\Gamma^o_{\Sigma+K^+}$ is a measure of the coupling of the resonance to the decay channel in question and the rest of the expression is the product of phase space, a barrier penetration factor, and form factor normalized to unity at the central mass M_o of the resonance. Both these latter factors depend strongly on the orbital angular momentum ℓ of the decay products. The X in the form factor is essentially the inverse of an effective range of interaction.[17]

The total width can be taken to be the sum of the energy dependent partial widths for all decay modes. In principle it is possible to determine both c and $\Gamma^o_{\Sigma^+K^+}$ by fitting. However since the Σ^+K^+ partial width is very small compared to the total width, the shape of the distribution is insensitive to the partial width and only the product $c\Gamma^o_{\Sigma^+K^+}$

is determined. We take the total width to be that obtained from pi-nucleon scattering data and $c\Gamma^{o}_{\Sigma^+K^+}$ then determines the percentage of resonance production in this reaction. We find 38 ± 5% of the events result from resonance production and 62 ± 5% from background. The parameter α is found to be .35 ± .05 $(BeV/c)^2$.

Determination of the rate of resonance production in the $\Lambda p K^+$ channel is rather more complicated. As mentioned above, there are three πp resonances near 1700 MeV. None of the branching ratios for decay into ΛK^+ is firmly known, nor have the relative production rates of these resonances been measured from non-strange particle production in p-p collisions. Some information about the parameters of these resonances has been obtained however from analysis of the differential cross section and Λ polarization in ΛK^o production in $\pi^- p$ collisions.[18] Reasonable agreement results with a J=5/2 resonance with parity either positive or negative, total width ~ 100 MeV and partial width into ΛK^o ~ 1-10 MeV. No analysis finds any evidence for the S-wave resonance in the ΛK^o system. Appeal to the requirement of SU_3 symmetry to determine branching ratios of the $5/2^+$ and $5/2^-$ N*'s are useless since both resonances are thought to be members of octets and their partial widths are sensitive functions of their D/F ratios. For example, a D/F ratio of 3 forbids decay into ΛK. The study of baryon resonances[19] suggests that this ratio is often widely different in different N* octets.

The data from this experiment are insufficient to determine the contributions of the various resonances. Since the associated production

data suggest a large J=5/2 amplitude we fit $d^2\sigma(\Delta^2,M^2)/d\Delta^2 dM^2$ to a single $F_{5/2}$ resonance at 1688 MeV together with a background contribution. As in the $\Sigma^+ nK^+$ case, we fit to an expression corresponding to (1) and find 54 ± 6% of the events result from resonance production and 46 ± 6% from background. The fitted value for α is .53 ± .03(BeV/c)^2. Use of a $D_{5/2}$ resonance gives an equivalently good fit with comparable fraction of resonance production.

In principle the angular distribution of the resonance decay products can provide the necessary information to determine the spin and parity of the parent state. In Fig. 14 we show the angular distribution, with respect to the momentum transfer direction, of the hyperon in the Σ^+K^+ c.m. system and in Fig. 15 that for the ΛK^+. Predictions of a π exchange model for production shown here with the experimental distributions will be discussed below. In both reactions the data in the resonance region are consistent with a resonance decay symmetric about 90° superimposed on a small asymmetric background. The spin density matrix of the resonance is not simply determined in proton-proton interactions, even for forward production. The possible angular distributions for high spin resonances are rather complex and with the limited statistical accuracy of the data it is not possible to identify the contributing states.

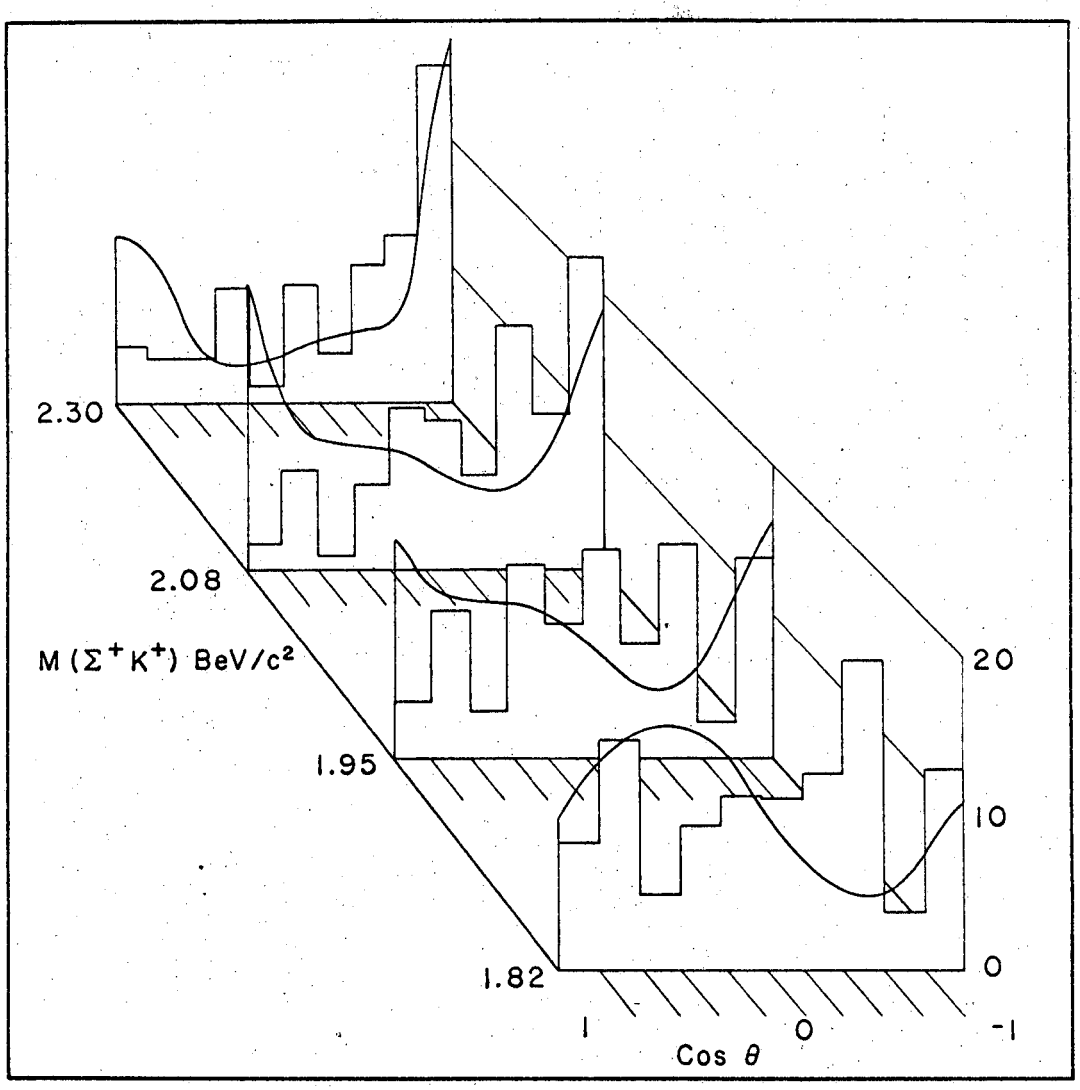

XBL676-3415

Fig. 14. Decay angular distribution of the Σ^+K^+ system produced in the channel Σ^+K^+n. The angle θ is between the Σ^+ and momentum transfer directions in the Σ^+K^+ rest system. The curves are predictions of pion exchange with a form factor.

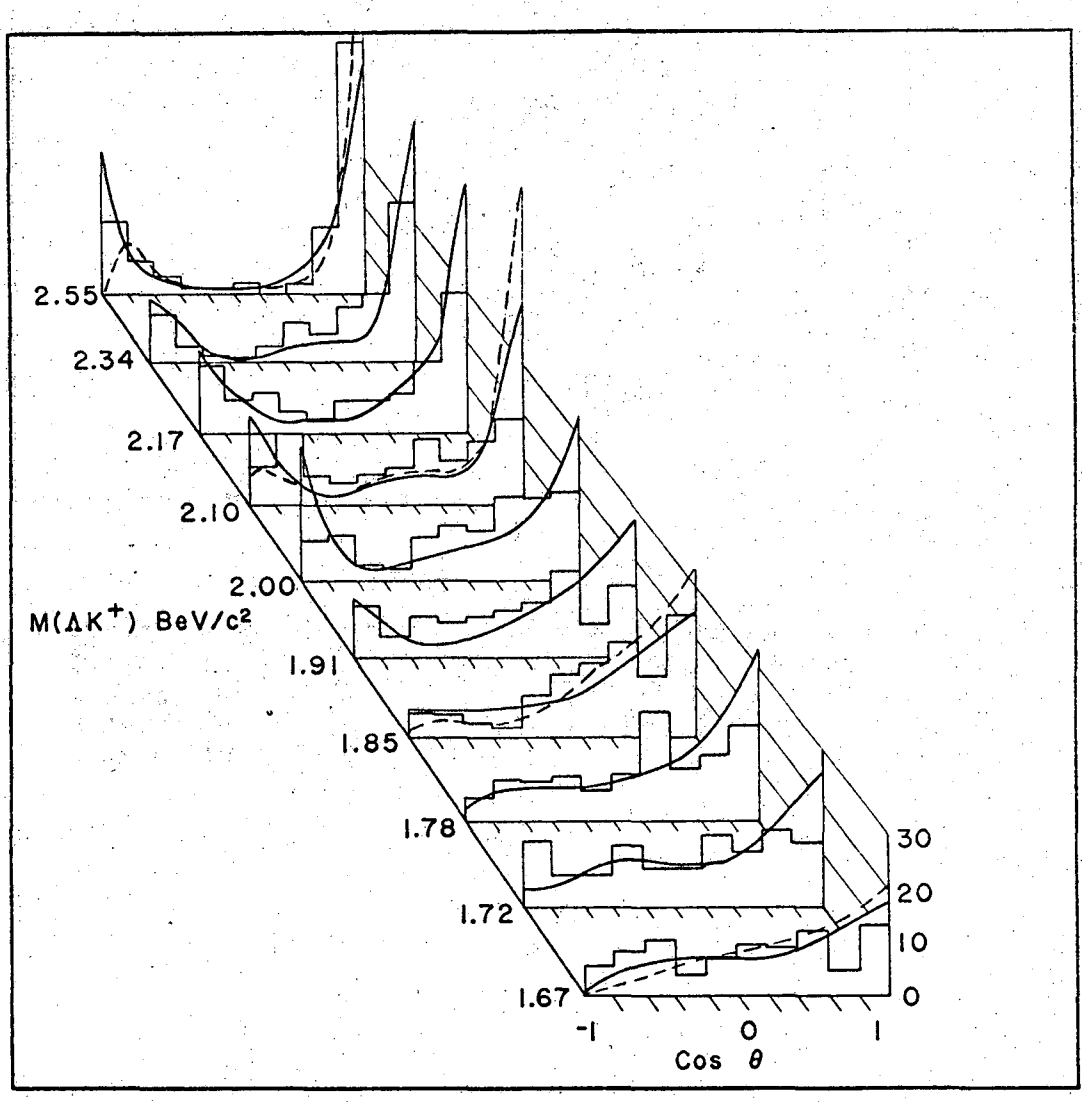

Fig. 15. Decay angular distribution of the ΛK^+ system. The angle θ is between the Λ and momentum transfer directions in the ΛK^+ rest system. The solid curves are predictions of pion exchange with a form factor. The dashed curves are pion exchange predictions with an interference contribution.

V. ONE MESON EXCHANGE MECHANISMS

A. General Features

As noted above the production angular distributions show the characteristic feature of peripheralism, a strong correlation between the final and initial state baryon directions. We display in Figs. 16 and 17 scatter plots of hyperon-kaon mass versus momentum transfer to the final state nucleon, showing the high concentration of events at small momentum transfers. We attempt to determine the compatibility of the data with predictions of simple models for peripheral production, in particular one particle exchange processes. Single particle exchange is by now well known as a theory of peripheral production. It is based on the assumption that low momentum transfer collisions are mediated by exchange of a single particle[20] and that the scattering amplitude is given by a single pole diagram as shown in Fig. 18 for $pp \rightarrow NYK$ reactions. One usually assumes that the vertex couplings and scattering cross sections involving the exchanged virtual particle do not change as the distance from the pole increases. There have been attempts to make "off the mass shell" corrections by using vertex form factors and relating cross sections involving real to those with virtual particles.[21] In addition, absorption and sharp cut-off schemes[22] for attenuating low partial-wave amplitudes are used to take initial and final state interactions into account and to correct the property that the simple model often violates unitarity for low partial waves.

For our reactions, the possibilities for exchange mechanisms are given by the diagrams in Fig. 18. For all channels but $pp \rightarrow \Sigma^+ K^+ n$,

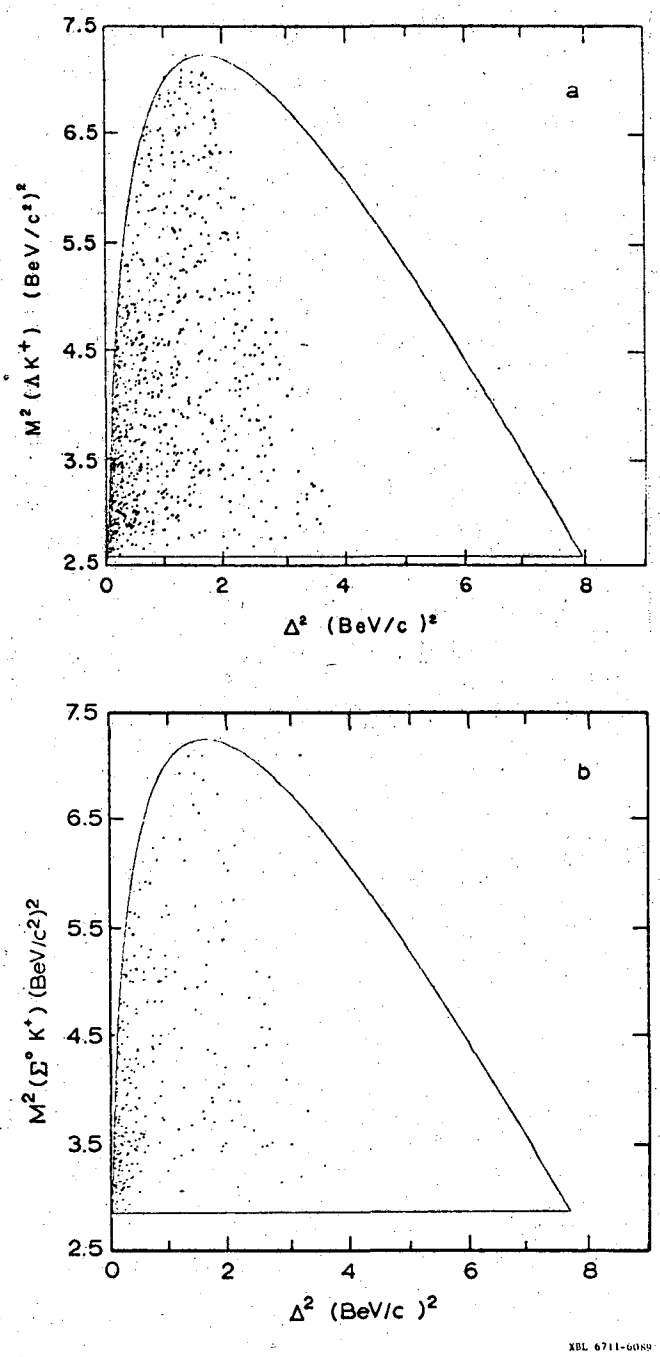

Fig. 16. Scatter plots of YK mass vs. momentum transfer to the nucleon: a. $pp \rightarrow \Lambda K^+ p$, b. $pp \rightarrow \Sigma^\circ K^+ p$.

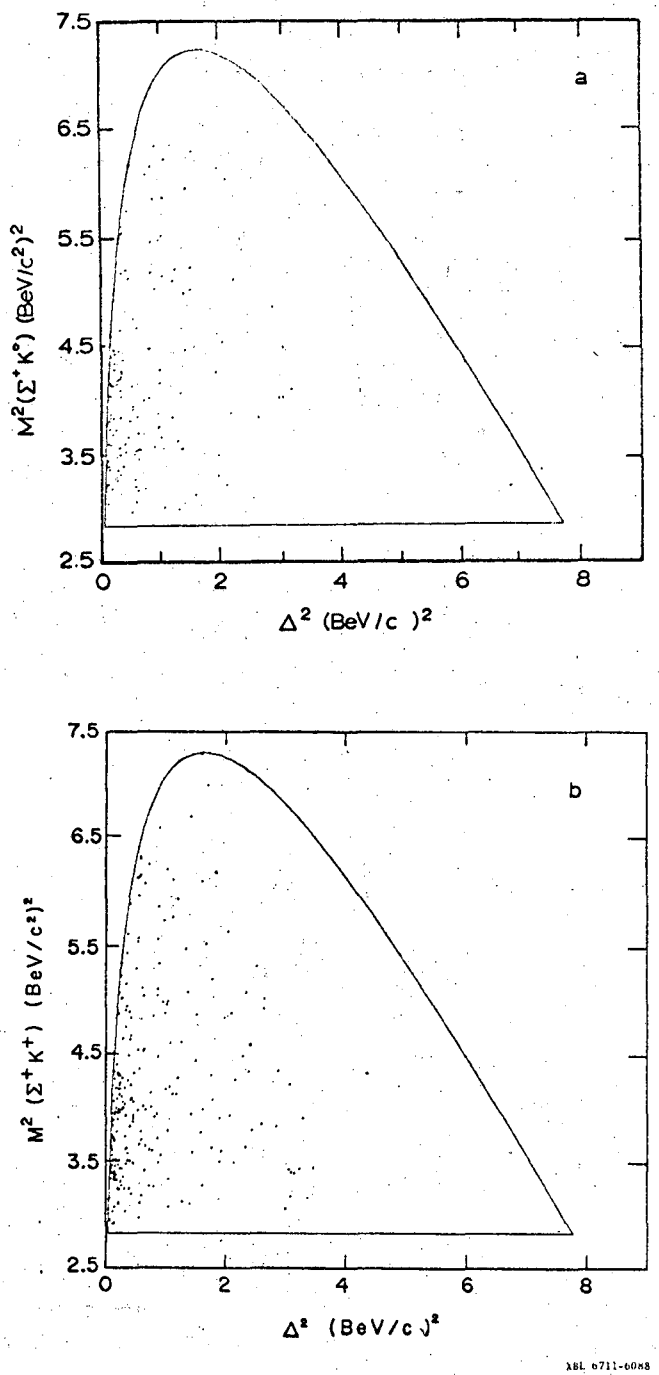

Fig. 17. Scatter plot YK mass vs. momentum transfer to the nucleon, (a) $pp \rightarrow \Sigma^+K^op$, (b) $pp \rightarrow \Sigma^+nK^+$.

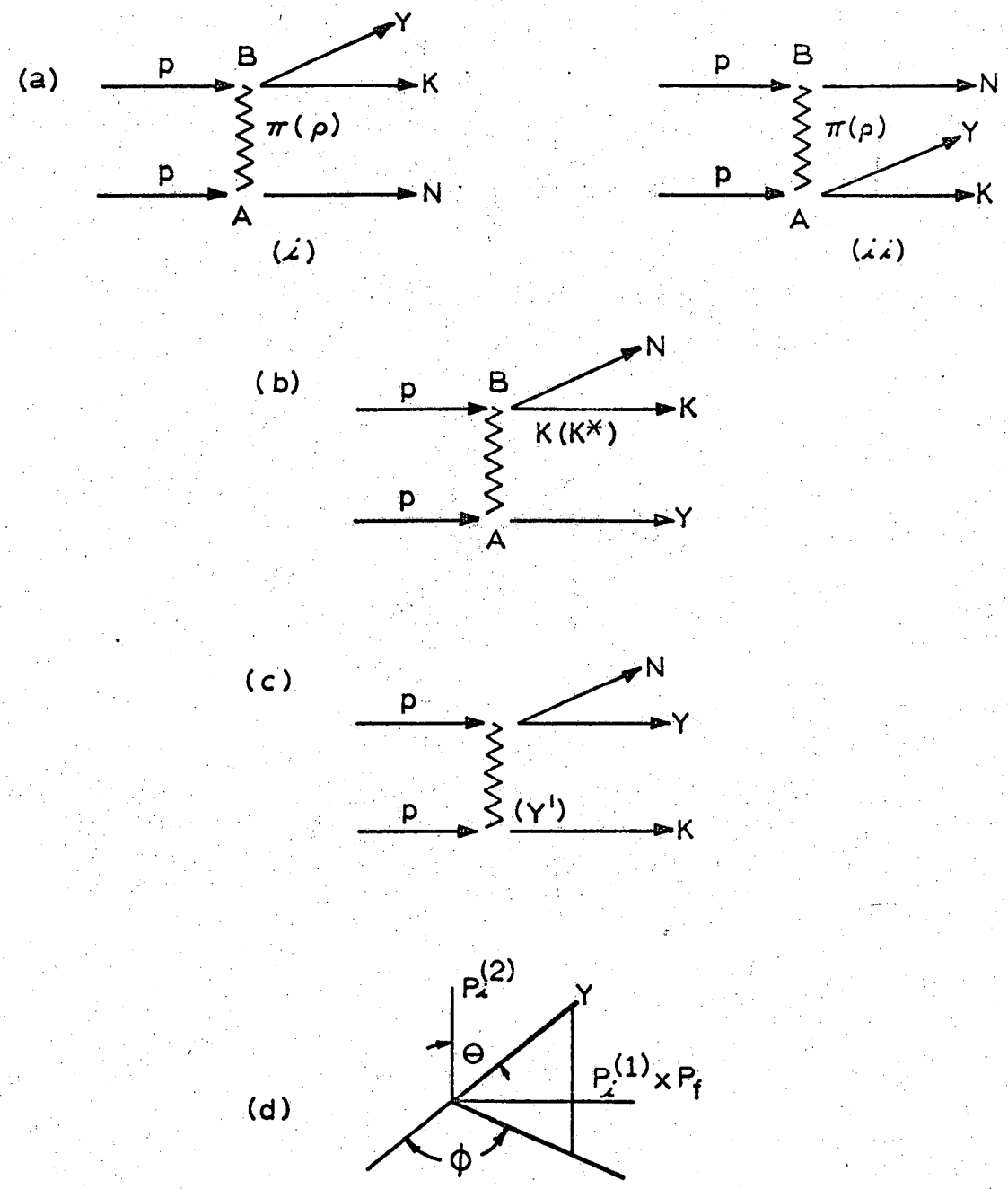

XBL6711 2112

Fig. 18. Single particle exchange diagrams for pp → YKN. (a) pion exchange, (b) kaon exchange, (c) baryon exchange. 18d defines the angles θ and φ. Particle symbols represent directions of motion in the YK center of mass frame.

ω and Φ exchange are possible as well but the large cross section for this reaction and the similarity of all the channels suggest that I=0 exchange is unimportant.

B. Pion and Kaon Exchange

We first examine pseudoscalar-meson exchange, making detailed comparisons of the predictions and data for the ΛpK^+ and $\Sigma^+ nK^+$ reactions and being somewhat more qualitative toward the other reactions. We have made calculations for the pion and kaon exchange models, using a Monte Carlo method, discussed in Appendix C, to generate events distributed according to:

$$\frac{d^4\sigma}{dM^2 d\Delta^2 d\Omega} = \frac{1}{4\pi}\,\frac{G^2}{4\pi}\,\frac{1}{(2\bar{p}\,\bar{E})^2}\,\frac{\Delta^2+(m_p-m')^2}{(\Delta^2+\mu^2)^2}\,k\,M\,\frac{d\sigma(M,\theta)}{d\Omega}$$

where

$$k = \frac{1}{M}\left[\frac{M^4}{4} - \frac{1}{2}M^2(m_p^2+\mu^2) + \frac{1}{4}(m_p^2-\mu^2)^2\right]^{1/2}$$

$\bar{p}$, $\bar{E}$ are the center-of-mass momentum and energy of the incident proton;

$\frac{G^2}{4\pi}$ = meson baryon-baryon coupling constant describing vertex A in Fig. 19;

we use $\frac{G^2_{pp\pi^o}}{4\pi} = 15$, $\frac{G^2_{p\Lambda K^+}}{4\pi} = 15$, $\frac{G^2_{p\Sigma^+ K^o}}{4\pi} = 0.64$; [23]

Δ^2 = four momentum transfer squared to the recoil baryon m' ; a nucleon for π exchange, Λ or Σ for K exchange;

μ = mass of exchanged meson, m_p = mass of proton;

M = invariant mass of the particles emerging at vertex B, e.g., YK for π exchange;

θ = angle between the momentum transfer $\vec{\Delta}$ and meson momentum in the YK or NK center-of-mass frame.

$\frac{d\sigma(M,\theta)}{d\Omega}$ is the differential cross section for the two-body production at vertex B,[24] $\pi p \to YK$ or K nucleon elastic or charge exchange scattering. We use only the strong interaction part of these cross sections since we never reach the small momentum transfers in the two-body system where Coulomb scattering is strong, though we parameterize with the angle θ.

k is a kinematic factor which can be identified as the three-momentum of the exchanged meson in the two-body center-of-mass frame.

The cross section (3) is the sum of squares of the two amplitudes related by interchange of the initial state protons and diagrammed in Fig. 18a. If we remove any distinction between the initial protons, (3) is just twice the cross section for one of the diagrams. It does not contain the interference term which can be computed only if one has knowledge of the relevant two-body scattering amplitudes. However, as discussed in Appendix B, we can place limits on the size of the interference contribution and we indicate interference contributions in the meson-exchange predictions. In Figs. 19a and 19b the solid curves show the predictions of π-exchange for the distribution in Δ^2 to the proton and K exchange for Δ^2 to the Λ respectively for reaction (a), where we plot the smaller of the two momentum transfers for each event. It is clear that in each case the experimental peak at small

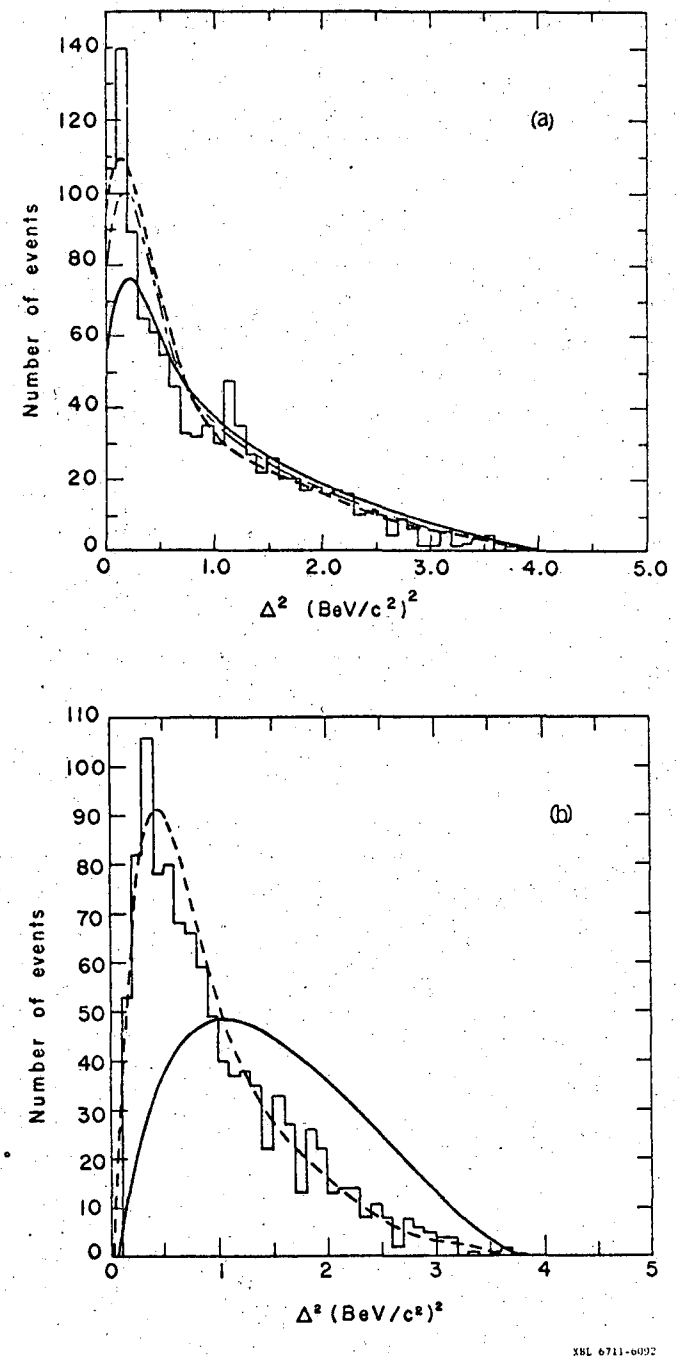

Fig. 19. (a) Distribution in momentum transfer to the final proton for $pp \rightarrow \Lambda pK^+$. The solid is the prediction of unmodified pion exchange and the dashed curves predictions with a form factor and containing two different treatments of interference. (b) Distribution in momentum transfer to the Λ. The dashed and solid curves are K exchange predictions with, and without a form factor. Theoretical curves are normalized to the experimental histograms.

values is considerably narrower than that predicted. This feature of stronger damping at large momentum transfer has been demonstrated often in many peripheral processes.[21] Most other features of the data are reasonably consistent with a single meson exchange mechanism and the momentum transfer discrepancy may be attributed to corrections to the model. In particular, absorption effects due to competing inelastic channels, vertex form factors, and off-the-mass shell corrections are known to modify the Δ^2 dependence given by the propagator and vertex term in the simple single-particle exchange process.[22] Since the momentum transfer distribution implies kinematic restrictions on the values other variables may assume, we include in further calculations a form factor, $F(\Delta^2)$, multiplying the above expression (3). The functional form, chosen so that the modified expression reproduces the dependence of the data on Δ^2 and is normalized to one at the relevant pole is:

$$F(\Delta^2) = \left(\frac{A - M_{exch}^2}{A + \Delta^2} \right)^2 .$$

For the pion-exchange case the fitted values for A, in reactions (a) through (d), are given in Table III. We note that A for the sigma channels lies between 1 and 2, while for the ΛpK^+ reaction it is 5. This property suggests that we are including in this form factor off-the-mass shell corrections at the associated production vertex and that the ΣK and ΛK cross sections behave differently as the incident pion becomes virtual. The dashed curves in Fig. 19 are meson exchange predictions with the form factor. The upper dashed curve of Fig. 19a

Table III. Total cross section predictions of π and K exchange.

Channel	$\Lambda K^+ p$	$\Sigma^o K^+ p$	$\Sigma^+ K^o p$	$\Sigma^+ K^+ n$
σ_{EXP} (μb)	54^{+3}_{-5}	17^{+4}_{-2}	29 ± 5	57 ± 7
$\sigma_{\pi\ EXC.}$ (μb) (unmodified)	96	107	99	414
A ($(BeV/c)^2$) (in π EXC. form factor)	5	1.9	1.3	1.8
$\sigma_{\pi\ EXC.}$ (μb) (modified)	62	37	35	164
$\sigma_{K\ EXC.}$ (unmodified)	3.2 mb	71 μb	143 μb[a]	53 μb
A ($(BeV/c)^2$) (in K EXC. form factor)	.72			.8
$\sigma_{K\ EXC.}$ (μb) (modified)	180 ± 100			$< 10 \pm 10$

(a) We use $K^+ p$ elastic data for this calculation since $K^o p$ elastic scattering cross sections have not been measured.

contains an interference contribution.

The most striking feature in each channel considered is the hyperon-kaon mass spectrum which must of course be reproduced by a relevant model. Predictions of both K-exchange and π-exchange are shown in Figs. 20 and 21 again with a measure of the interference uncertainty. For reactions (a), (c) and (d) the π-exchange model satisfactorily reproduces the peaks in the ΛK and ΣK spectra while agreement with the K-exchange model is poor. Agreement with π-exchange is not as good for reaction (b), though still much better than for K-exchange. The data sample for this reaction suffers from the ambiguity problem discussed above. In addition, to obtain the $\pi^o p \to \Sigma^o K^+$ cross section, we use the isotopic spin equality relating it to cross sections for $\pi^- p \to \Sigma^o K^o$, $\Sigma^- K^+$ and $\pi^+ p \to \Sigma^+ K^+$ reactions. Because these reactions differ experimentally, there could be a systematic error in their relative normalization, causing a poorly calculated π-exchange prediction. The total cross sections calculated from the unmodified π-exchange and K-exchange models as well as those predicted with the addition of the form factor are given in Table III. There is considerable uncertainty in the modified K-exchange predictions, due to the inadequacy of a one-parameter form factor, which appears as a lack of reproducibility for these predictions when different functional forms for $F(\Delta^2)$ are tried. Both the modified and unmodified π-exchange predictions are in better agreement with the experimental data than the corresponding K-exchange predictions. As a further test of the model, we examine the Λ polarization obtained from the angular distribution of the decay products

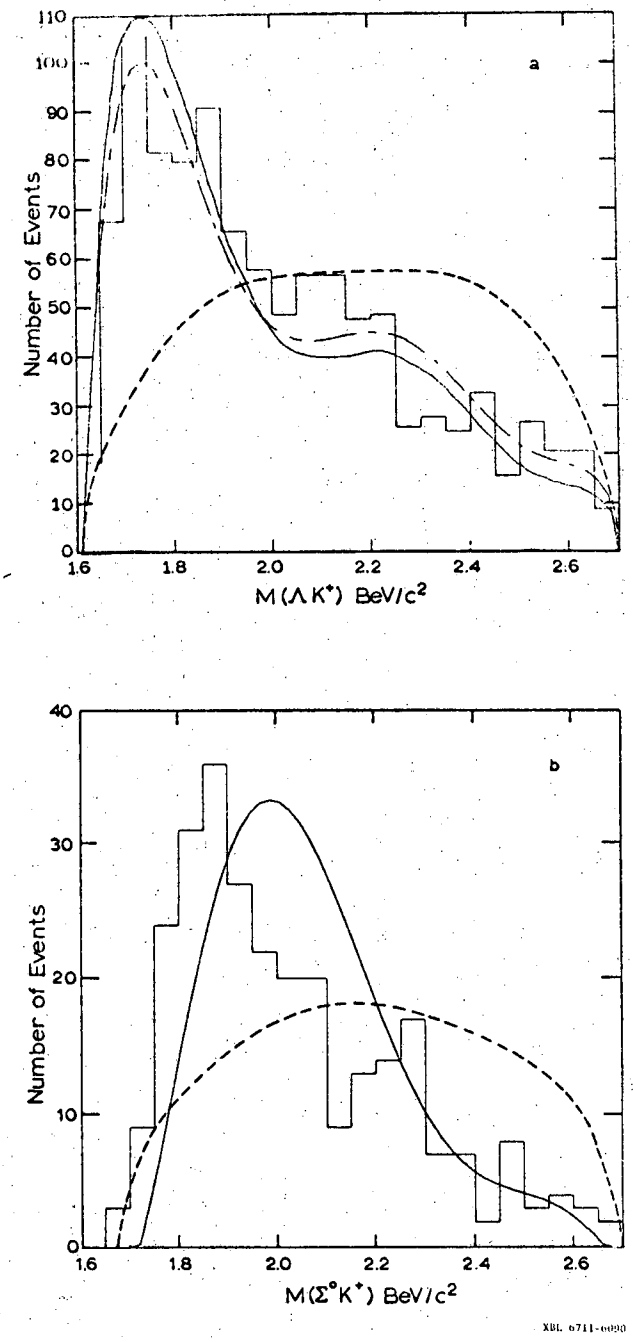

Fig. 20. YK mass distributions for (a) $pp \rightarrow \Lambda pK^+$ and (b) $pp \rightarrow \Sigma^o pK^+$. Solid curves are modified pion exchange predictions and dashed curves unmodified K exchange predictions. Fig. 20a shows a second pion exchange curve containing an interference contribution.

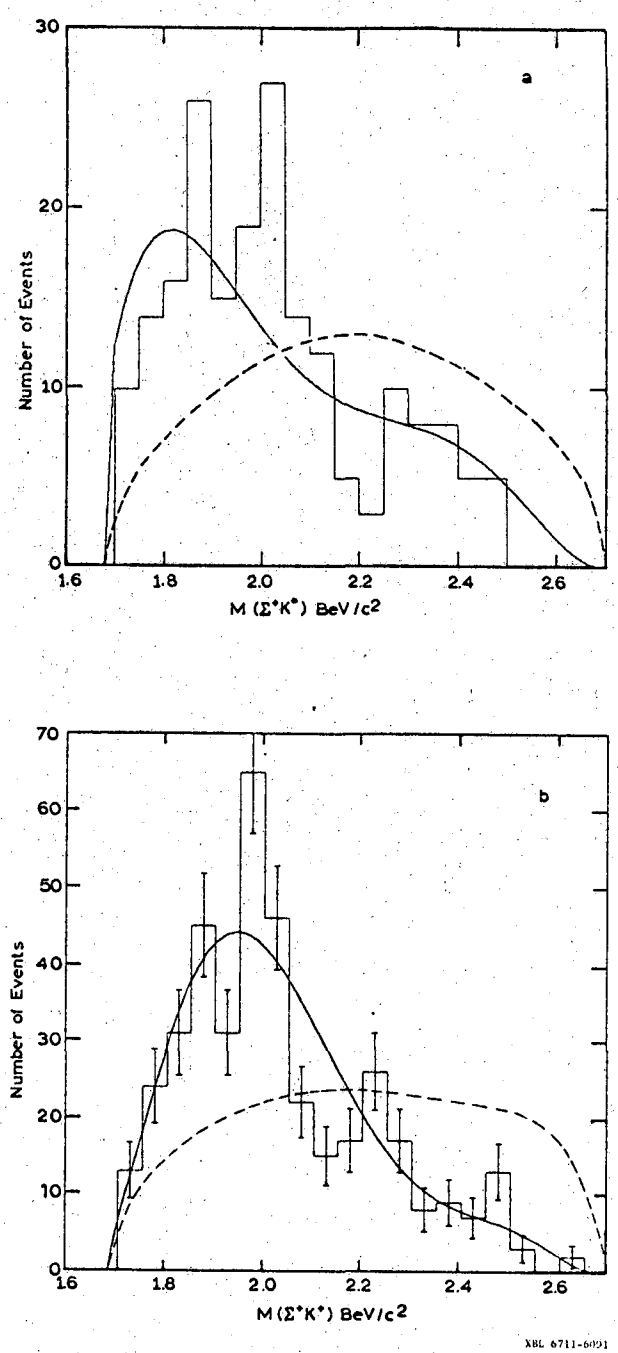

Fig. 21. YK mass distributions for (a) $pp \rightarrow \Sigma^+ pK^o$ and (b) $pp \rightarrow \Sigma^+ nK^+$. Solid curves are modified pion exchange predictions and dashed curves unmodified K exchange predictions.

of the Λ in its rest frame. The polarization is measured along the normal to the plane containing the directions of the Λ and relevant initial proton in the ΛK^+ center-of-mass system. We show in Fig. 22 experimental values for the Λ polarization averaged over intervals in ΛK^+ mass, together with the predictions of pion exchange. Considerable polarization is noted, particularly at low momentum transfer and low ΛK^+ mass, in agreement with the results obtained for the associated production reaction $\pi^- p \to \Lambda K^o$. The K-exchange model predicts zero polarization since only a p-wave Λ production amplitude is present. Thus we find the data consistent with that expected for a dominant pion exchange mechanism with no evidence for a contribution from K exchange.

We now study the predictions of the π-exchange model for distributions in the angles θ and φ, defined in Fig. 18d, in reactions (a) and (d). Figures 14 and 15 show the angular distribution of the Σ^+ and Λ in the YK^+ center-of-mass system, with the momentum transfer as polar axis, together with the π-exchange predictions. Agreement is very satisfactory. In Figs. 23 and 24 we show distributions in the Treiman-Yang angle, φ, and observe a substantial lack of isotropy except at very small Δ^2 where kinematics constrains the distribution to be isotropic.

Some deviation from isotropy is expected to result from our choice of the smaller momentum transfer in the definition of φ. The modified pion exchange calculation shows that for nine percent of the events, our computed value of φ is that one appropriate to the exchange

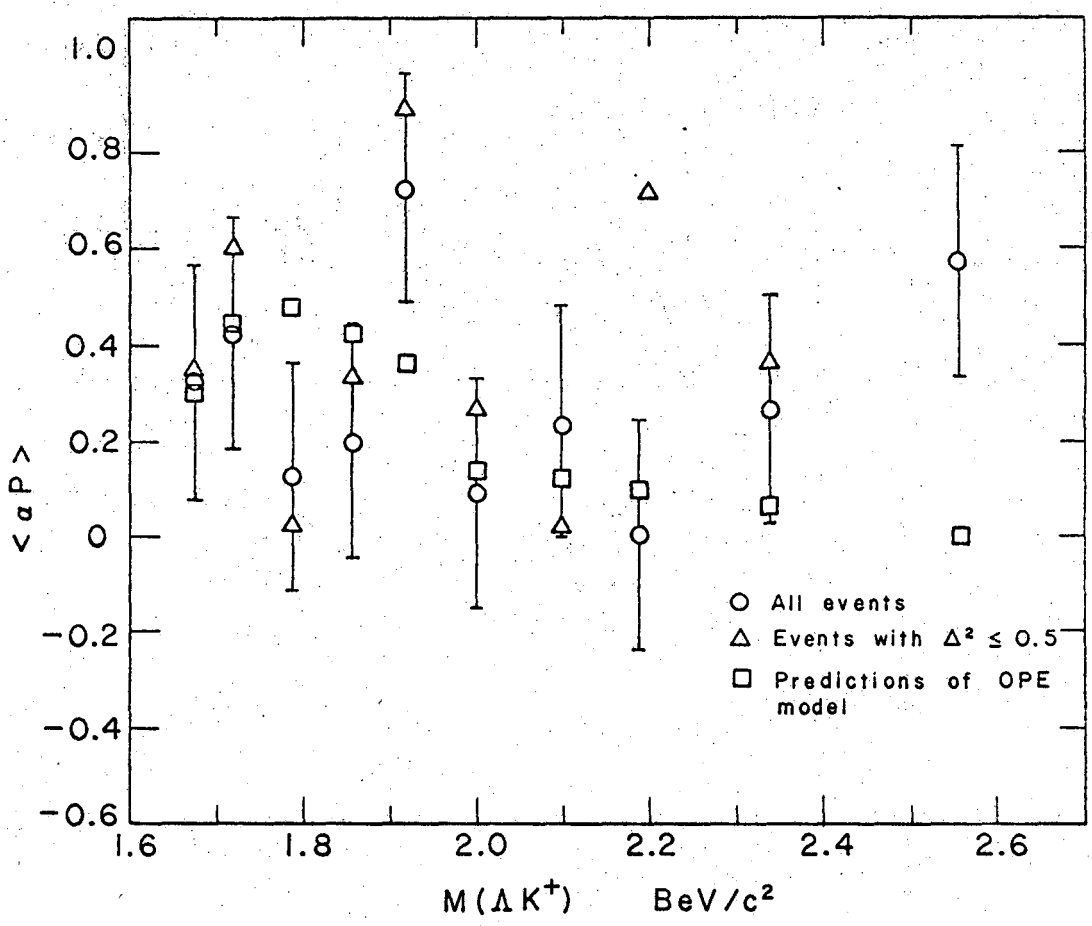

Fig. 22. Lambda polarization for the reaction $pp \rightarrow \Lambda pK^+$ as a function of ΛK^+ mass. Polarizations for small momentum transfer events and pion exchange predictions are shown.

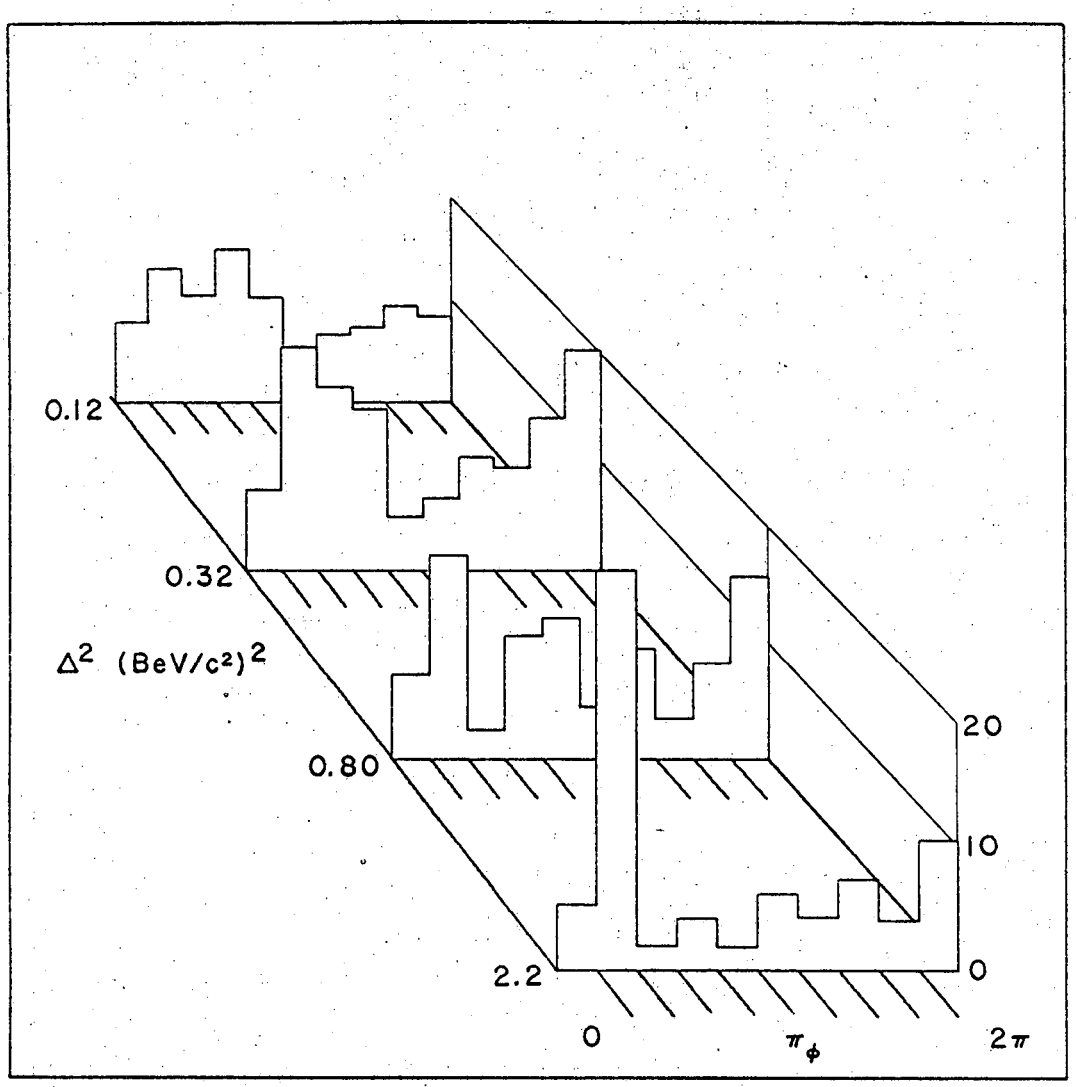

XBL676-3412

Fig. 23. Treiman-Yang angle distribution for the reaction $pp \rightarrow \Sigma^+ K^+ n$ as a function of momentum transfer.

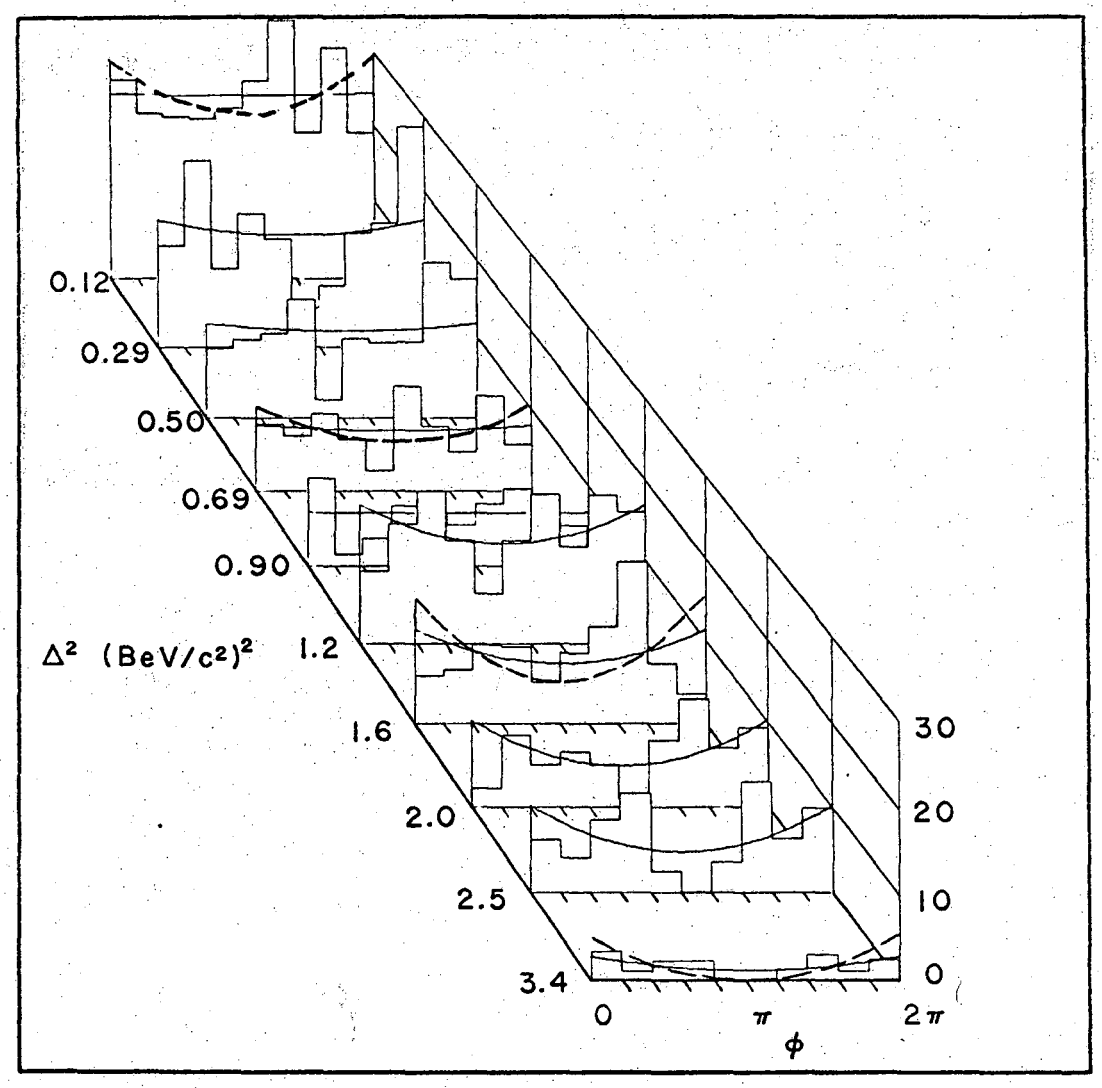

XBL676-3416

Fig. 24. Treiman-Yang distribution for the reaction $pp \rightarrow \Lambda pK^+$ as a function of momentum transfer. The smooth curves are predicted by pion exchange and are normalized to the experimental histograms. The dashed curves contain an interference contribution.

diagram and these events are not distributed isotropically. The curves on the figures contain this effect which clearly does not explain the magnitude of the experimental anisotropy.

A larger effect can be generated by the interference term, which as seen in Appendix B, is of the form $d\sigma = (A + B \cos \varphi)d\varphi$, where A and B are functions of the associated production amplitudes and have weak dependences on φ. The solid curves in Fig. 23 are the pion exchange predictions without any interference and the dashed curves are predictions which maximize the possible asymmetry due to interference. It appears that we can in this way account for our experimental anisotropy, at least moments in cos φ in the Treiman-Yang distribution. Small cos 2φ moments also appear to be present qualitatively and it is difficult to generate these with single pion exchange.

We plot total $pp \rightarrow \Lambda pK^+$ cross sections[25] from a number of experiments at various beam momenta in Fig. 25. Curve a is the prediction of unmodified pion exchange and curve b that for pion exchange with a form factor. Both predictions, as well as the experimental cross section, rise rapidly above threshold but then have a very smooth momentum dependence. The measured cross section becomes rather constant at about 55 μb, lower than the corresponding values of both predictions, which are ~ 100 μb and ~ 70 μb respectively. However the magnitude of the interference contribution to the predicted total cross section at 6 BeV/c can be as large as 8 μb and a large constructive interference at all momenta above 3 BeV/c could bring the data and modified pion exchange predictions into fairly close agreement. If we parameterize

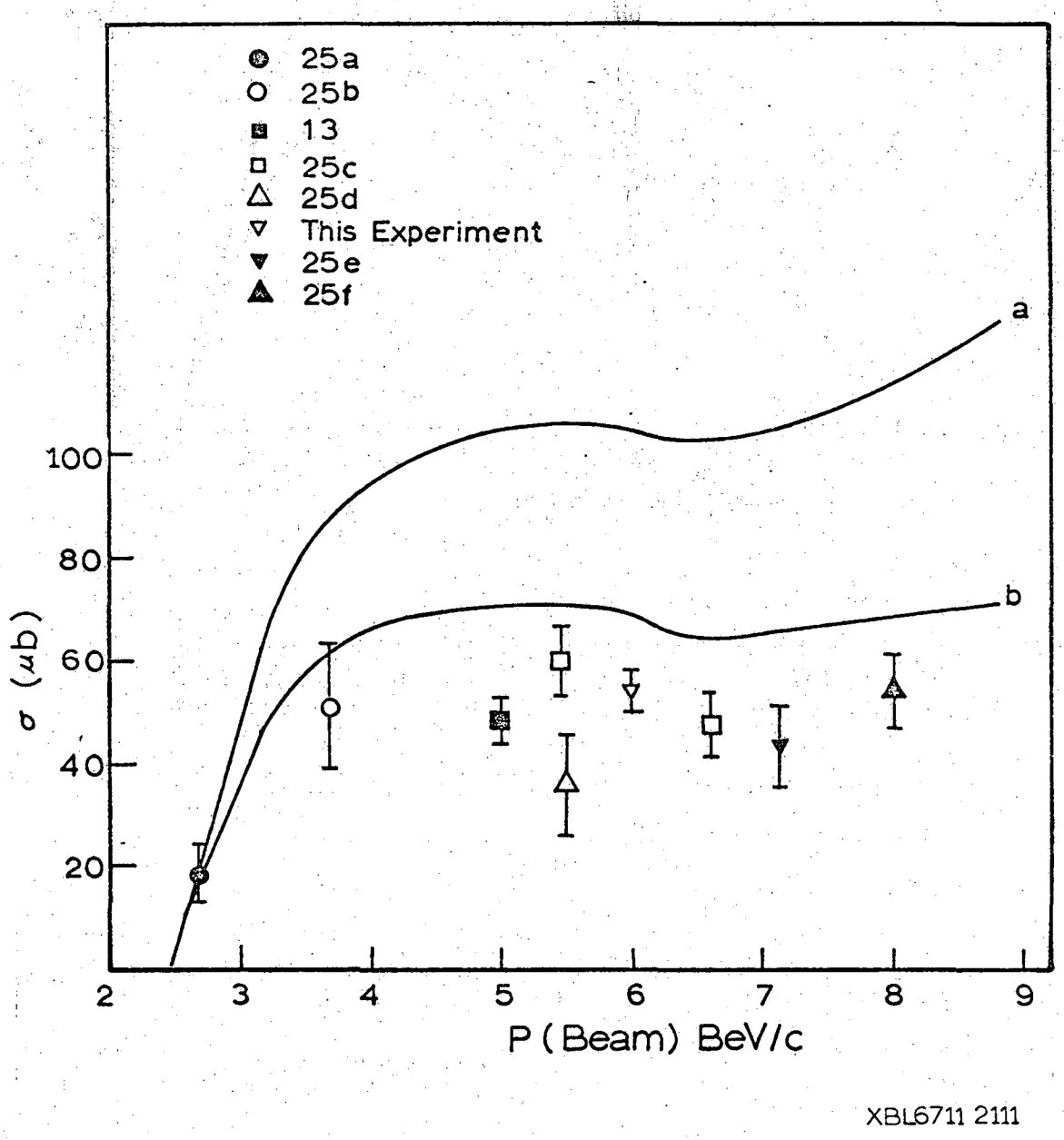

Fig. 25. Total cross sections for $pp \rightarrow \Lambda pK^{+}$. Curve a is the prediction of unmodified pion exchange and curve b is that for pion exchange with a form factor.

the momentum dependence of these cross sections by $\sigma = C\ p^{-n}$ we find that n can be as large as 1.1 between 5 and 7 BeV/c but is < 0.4 if one uses the entire range above 3.5 BeV/c. In the scheme of Ref. 5, this momentum dependence is consistent with diffraction and non-strange meson exchange, and certainly inconsistent with strange meson and baryon exchange.

We conclude that the single pion exchange mechanism with a form factor is in reasonable agreement with the data. A more detailed analysis, involving absorbtive corrections and an exact treatment of interference is necessary to determine whether the apparent discrepancies such as the sharp momentum-transfer peak and Treiman-Yang angle anisotropy can be accomodated. Unfortunately, the complete lack of information about absorption in the final state and associated production amplitudes makes such calculations impossible.

C. Other Exchange Mechanisms

The exchange of ρ and K* mesons is another model which could naturally reproduce the features of our data. In particular, it is well known that vector meson exchange gives rise to cos φ and cos 2φ moments in the Treiman-Yang angle distribution as well as correlations between φ and θ, the two-body scattering angle.[21] Our data does show a correlation of this kind, the anisotropy in φ being strongest at small θ for the non-strange meson exchange coordinate system.

Again, as in the pseudoscalar mesons case, it is improbable that K* exchange can give rise to sharp peaks in the YK mass spectra. since no explicit YK interaction is contained in the model. The

exchange of ρ mesons is a good candidate for the mechanism in these reactions but the fact that the $\rho + p \rightarrow Y + K$ cross section is unphysical makes a full calculation impossible. The analysis of Stodolsky and Sakurai[26] indicates that the ρ nucleon and γ nucleon interactions are similar. It would be reasonable to attempt a ρ-exchange calculation with photo-production data. However very little data is available for the reactions $\gamma + N \rightarrow Y + K$ and such a calculation is not possible yet. A remaining possibility is to consider the events produced by $p + p \rightarrow N^* + N$ and fit to a parameterization of the ρ exchange cross section, requiring four parameters, one of which is a normalization to the cross section. However, there is a great deal of background under our resonance peaks and the quantum numbers of the resonance in the $\Lambda K^+ p$ reaction are quite indefinite. Further, we will again have to modify the momentum transfer dependence given by the model, since ρ exchange will give a prediction even broader than that of unmodified pion exchange. We feel that it is not possible to compute a meaningful ρ exchange prediction although it is likely that a small amount of ρ exchange would improve the agreement of the Treiman-Yang distribution with the one-meson exchange model.

A study of ρ exchange would be much more useful if the ρNN vertex coupling were known as well as the ρNN^* appears to be from the Stodolsky-Sakurai analysis. We could then reduce by two the number of parameters in a fit to the cross section. A suitable reaction for the study of this coupling is $\pi^- p \rightarrow n\omega$, where isoscalar and π exchange are forbidden. Experimentally, this cross section has not been studied sufficiently to provide

this information.

We finally consider Regge exchange. Data for N* production in non-strange particle states produced in p-p interactions,[27] as well as the $pp \rightarrow \Lambda pK^+$ data given above shows that total cross sections slowly with total energy, above a beam momentum of a few BeV/c. In addition, production is very peripheral for all of these processes. The data suggest that Pomeranchon exchange may contribute to these reactions at intermediate energies. As for vector meson exchange, one can parameterize the Regge-pole couplings to the nucleon-nucleon and nucleon-N* systems, and fit the resonance production data to the prediction. One encounters just the difficulties discussed above; background, a large number of parameters, as well as the likelihood that a single Regge pole is not sufficient, since in p-p elastic scattering at least three appear to be required.[28] We have chosen not to pursue a Regge analysis of the data.

VI. TEST OF SU_3 PREDICTIONS

It is often possible to use a symmetry such as SU_3 to relate a number of amplitudes A_i for reaction channels to a smaller number of amplitudes which characterize the symmetry. In such a case one derives a set of independent relations of the form

$$\sum_i C_i A_i = 0 \quad .$$

Each such relation provides a set of inequalities

$$\sum_{i=j} |C_i A_i| \geq |C_j A_j|$$

which may be experimentally tested by using

$$|A_i| = \sqrt{\sigma_i / \rho_i}$$

where σ_i is the relevant differential channel cross section and ρ_i is a phase space factor.

We consider the relations implied by exact SU_3 symmetry for the reactions $pp \to BBP$ where B is a member of the baryon octet and P is a member of the pseudoscalar meson octet. The initial state transforms like the $I = I_3 = 1$, $Y=2$ member of the 27 dimensional representation of SU_3 and there are six independent ways to couple 3 octets to an object with these transformation properties. These correspond to the six permutations of particle labels in the coupling $\chi_1^\alpha(1)\ \chi_\alpha^3(2)\ \chi_1^3(3)$ where $\chi(1)$ and $\chi(2)$ represent the baryons and $\chi(3)$ represents the meson. Thus there are six amplitudes characterizing the reactions and twelve channel amplitudes. Reference 29 discusses the way in which relations among the

A_i may be systematically obtained from a system of equations involving SU_3 invariant reaction amplitudes. In this case we are led to four equations. They are:

1. $\sqrt{2}\ p\ \Sigma^{o}K^{+}(\vec{x}) - n\Sigma^{+}K^{+}(\vec{x}) - p\Sigma^{+}K^{o}(\vec{x}) = 0$

2. $pn\pi^{+}(\vec{x}) + np\pi^{+}(\vec{x}) - \sqrt{2}\ pp\pi^{o}(\vec{x}) = 0$

3. $-p\Sigma^{o}K^{+}(\vec{x}) + \sqrt{2}\ \Sigma^{+}nK^{+}(\vec{x}) + \sqrt{3}\ p\Lambda K^{+}(\vec{x}) + \sqrt{2}\ pn\pi^{+}(\vec{x}) = 0$

4. $2p\Sigma^{+}K^{o}(\vec{x}) + 2\Sigma^{+}pK^{o}(\vec{x}) + \sqrt{2}\ pp\pi^{o}(\vec{x}) + \sqrt{6}\ pp\eta(\vec{x}) = 0$

where $\vec{x}$ is a set of momentum and spin variables specifying the reaction.

We are interested, however, in comparing total channel cross sections. We must make the assumption

$$\int_{\substack{\text{spins}\\ \text{and}\\ \text{momenta}}} \frac{\sigma_i(\vec{x})}{\rho_i(\vec{x})}\, d\vec{x} \sim \frac{\sigma_i}{\rho_i}$$

where σ_i and $\rho_i = \int \rho_i(\vec{x})d\vec{x}$ are the total cross section and total phase space for the channel i. We thus derive inequalities among total cross sections which approximate the effects of kinematical differences between channels. They are

$$\sum_{i=j} |c_i| \sqrt{\frac{\sigma_i}{\rho_i}} \geq |c_j| \sqrt{\frac{\sigma_j}{\rho_j}} \ .$$

For inequalities involving reactions related to one another by I-spin transformations the phase space factors may be dropped. They may also be dropped if mass differences within SU_3 multiplets are small.

Table IV gives cross sections measured in the experiment as well as some measured at 5.5 BeV/c for reaction cross sections not yet determined in our experiment. For those channels in which cross sections have been

Table IV. Three-body channel cross sections and phase space factors for pp reactions at 5.5 and 6 BeV/c.

Channel	σ(mb)	ρ(relative)	$\sqrt{\sigma/\rho}$
ΛpK^+	.054 ± .004	1.0	.23 ± .02
$\Sigma^o pK^+$	.017 ± .003	.868	.14 ± .02
$\Sigma^+ pK^o$	.026 ± .004	.868	.172± .02
$\Sigma^+ nK^+$	.057 ± .007	.868	.256± .03
$pp\eta$	.030 ± .010 (a)	1.23	.156± .06
$pn\pi^+$	8.0 ± .2 (b)	1.828	2.09 ± .05
$pp\pi^o$	2.77 ± .1 (b)	1.828	1.23 ± .045

(a) Determined in this experiment from non-strange four-prong data.

(b) 5.5 BeV/c cross sections for Reference 24d.

determined for in both experiments they are equal to within two standard deviations.

We now apply the inequalities implied by relations 1-4 above. Relation 1 implies a triangle inequality which is well satisfied, the sides of the triangle having relative lengths .204, .261, .17 respectively. For relation 2 we note that the $pp\pi^o$ amplitude is correctly anti-symmetrized and

$$\sigma_{pp\pi^o} = \int_{|\vec{p}_1| \geq |\vec{p}_2|} \sigma(\vec{p}_1, \vec{p}_2, \pi^o) d\vec{x} \quad \text{then} \quad \sqrt{\frac{\sigma}{\rho}_{pp\pi^o}} \sim \frac{1}{\sqrt{2}} \sqrt{\int \frac{\sigma(\vec{x})}{\rho(\vec{x})} d\vec{x}}$$

and the inequality becomes $\sigma_{pn\pi^+} \geq \sigma_{pp\pi^o}$. This relation is satisfied, the left and right sides are 8 mb and 2.77 mb.

Relations 1 and 2 are implied by isotopic spin conservation alone and are expected to be in agreement with the data.

Relations 3 and 4 relate strange and non-strange particle production and are a test of the extent to which SU_3 is broken in these three-body production reactions.

The terms in the set of inequalities specified by relation 3 are respectively .14, .36, .40, 2.95. The inequality with the channel $pn\pi^+$ on the right is not satisfied, the left and right side having magnitudes .80 ± .10 and 2.09 ± .09 respectively. Finally relation 4 implies a triangle inequality among the terms

$$2\sqrt{\frac{\sigma}{\rho}\, p\Sigma^+K^o} \quad , \quad \sqrt{\frac{\sigma}{\rho}\, pp\pi^o} \quad , \text{ and } \quad \sqrt{3\,\frac{\sigma}{\rho}\, pp\eta} \quad .$$

The relative magnitudes of these expressions are .34 ± .02, 1.2 ± .05, and .27 ± .1 . Again in this case the data are not consistent with the inequality, the single pion production cross section being too large.

There are considerable uncertainties in our method of making phase space corrections and going from differential to total cross sections. However the rather violent disagreement between the SU_3 predictions and experimental cross sections suggests a real inaccuracy in the amplitude relations of unbroken SU_3. In the absence of a dynamical model it is hard to estimate the extent of the symmetry breaking and relate it to that generating mass differences within multiplets. However we conclude that it is an important factor in these reactions.

VII. CONCLUSIONS

Three-body strange particle states produced in proton-proton interactions proceed dominantly through the pion exchange mechanism. There is considerable nucleon isobar production and these isobars, the $N^*_{3/2}(1920)$ and $N^*_{1/2}(1688)$ have properties consistent with those inferred from pion-nucleon scattering.

No evidence was found for the existence of a resonant hyperon-nucleon state with mass within the limits

$$2.05 \leq M_{\Lambda p} \leq 3.14 \text{ BeV}/c^2$$

$$2.15 \leq M_{\Sigma^+ n} \leq 3.14 \text{ BeV}/c^2 \quad .$$

ACKNOWLEDGMENTS

I am most grateful to Professor William Chinowsky, who guided this work and provided counsel throughout my graduate career.

I am indebted to Professor Jonas Schultz for his close supervision and warm encouragement, as well as his seemingly unlimited hospitality.

My thanks go to Mr. Robert Kinsey and Mr. Stanley Klein, who worked ably with me on this experiment.

I thank Dr. Martin Perl and Dr. Tai Ho-Tan and their group of scanners at SLAC, who shared the work on this experiment.

I thank Professor Emilio Segrè for his support of this work.

I am grateful to Mr. William Gage, Mr. Bruce Douglass, and Mrs. Judy Conklin whose programming and bookkeeping efforts made this experiment possible.

Many thanks are due to the scanners and measurers who worked on this experiment.

I appreciate the help of Mrs. Rosemary Fowell for typing this thesis as well as for her many other contributions to this work.

This work was performed under the auspices of the U. S. Atomic Energy Commission.

APPENDICES

A. Corrections for Data-Processing Inefficiencies

Each of the reactions studied contains one or more unstable particles, Σ^+, Λ, Σ^o or K^o, in the final state. Since the decay properties of the particles are well established, we can determine the efficiencies for scanning and processing events with decaying particles. In particular, an unbiased sample of Σ^+, Λ, or K^o must show a decay (proper time) distribution of the form

$$F(t) = Ce^{-t/\tau_o}$$

where τ_o is the relevant lifetime. The rest frame decays of K^o and Σ^o must be isotropic since the K^o is spinless, and the Σ^o decay, a $\frac{1}{2}^+ \rightarrow \frac{1}{2}^+ + \gamma$ transition. We describe the unit momentum vector $\hat{P}_D$ of the decay product in the decaying particle rest frame with respect to the particle's direction $\hat{P}$ by a polar angle θ_R, where $\cos\theta_R = \hat{P}_D \cdot P$, and an azimuthal angle ϕ_R. Then the distribution in $\cos\theta_R$ for the Σ^+ and Λ must be uniform since there may be no polarization in a plane containing the decaying particle. A polarization normal to the production plane will give rise to an anisotropy in ϕ_R, but if the production planes are uniformly distributed about the beam direction, this anisotropy will vanish as well. Since α for the $\Sigma^+ \rightarrow n\pi^+$ decay is very near 0, there must be no significant anisotropy in ϕ_R for even a given production plane orientation in this process.

The decay time distributions for Λ, Σ^+, K^o show severe depletion at small values but have the correct shape and slopes beyond $t \sim .3 \times 10^{-10}$ sec.

The rest frame decay angle distributions of the Σ^o, Λ, and K^o are quite consistent with isotropy when summed over all production configurations. However the $\Sigma^+ \rightarrow n\pi^+$ and $\Sigma^+ \rightarrow p\pi^o$ events show considerable depletions. near $\cos \theta_R = \pm 1$.

We attribute these depletions to scanning and processing inefficiency for certain event configurations, those in which the decay occurs so close to the production vertices, or if a Σ^+ decay, at such a small angle to the Σ^+ direction, that the event is either not observed by the scanner or is measured badly.

We correct for such inefficiency by rejecting those events which do not lie within a specific range of projected track length and decay angle and weighting the remainder by the inverse of the probability for their having occurred within this region. We chose the minimum and maximum projected lengths and angles by examining the behavior of the total weighted numbers of events as these cutoff values are varied. The goal is to choose the least restrictive cuts for which no severe losses of events are indicated, by stopping at the point where more restrictive cuts do not further increase the weighted totals. The values chosen are given in the text and are such that no regions kinematically accessible to the unstable particles are excluded. In no case are more than 65% of the events excluded by the cuts, the worst case that of high momentum Σ^+'s.

Length selection and weighting

We consider an unstable particle of mass M, mean lifetime τ_o, lab momentum p and dip angle λ. If we demand that the projected length ($\ell^P = \ell^{space} \times \cos\lambda$) lie inside the interval $\ell^{min} < \ell^P < \ell^{max}$, the probability of observing the decay is

$$P(p,\lambda) = e^{\frac{-\ell_{min} M}{pc\tau_o \cos\lambda}} - e^{\frac{-\ell_{max} M}{pc\tau_o \cos\lambda}}$$

To correct for those events in which the unstable particle decayed outside the specified length interval, we assign the weight $W_L = 1/P(p,\lambda)$ to each accepted event.

For the cases of Λ and K^o decay, in which the average decay length is comparable to the chamber dimensions, ℓ_{max} is taken to be the distance along the neutral from the production vertex to the fiducial volume boundary, and ℓ_{min} is taken to be 1.5 cm. The Σ^+ decays suffer from K^+ and π^+ contamination if long candidates are accepted and ℓ_{max} and ℓ_{min} were taken to be 22 cm. and 1.1 cm. respectively. The average weight factor due to decay length for events with Λ, K^o, Σ^+ are respectively 1.3, 1.3 and 1.4.

Angle selection and weighting

It is necessary also to set a minimum and maximum produced projected decay angle cutoff for Σ^+ decays. Study of the $\Sigma^+ \to n\pi^+$ decays leads to a minimum angle of 10^o and a maximum of 75^o. Since the $p\pi^o$ decay of a Σ^+ with momentum greater than 1.4 BeV/c necessarily occurs with a decay proton angle smaller than 10^o, the proton decays must be

eliminated from the sample. Actually this decay mode is so severely depleted that it comprises only about 25% of the Σ^+K^+n events anyway. The maximum pion decay angle at the upper Σ^+ momentum, 5.3 BeV/c, is 18° and 55% of the pion decay events at this momentum survive the 10° minimum angle requirement.

The weight assigned to each surviving event is computed as follows: The probability for decay into the specified region is the available solid angle in the decaying particle's rest frame divided by 4π.

$$P_A(p_\Sigma,\lambda_\Sigma) = \frac{\int d\Omega_R \text{ (allowed by cuts)}}{4\pi}$$

The boundaries giving the integration volume in the decaying particle rest frame are determined by solving the equations relating the laboratory angles to rest frame angles, where β is the laboratory projected angle

$$\text{Tan}(\beta_{min}) = \frac{p_\pi \sin\theta_R \sin\phi_R}{\frac{E_\Sigma}{m_\Sigma}(p_\pi \cos\theta_R + \frac{p_\Sigma}{E_\Sigma} E_\pi)\cos\lambda_\Sigma - p \sin\theta_R \cos\phi_R \sin\lambda_\Sigma}$$

and an identical equation for $\text{Tan}(\beta_{max})$.
These are quadratic equations for ϕ_R and their solution permits easy numerical evaluation of the intergral above. The total weight for a decaying Σ^+ is then $W = W_L \times W_A$ where $W_A = 1/P_A$. The average W_A for an event with a Σ^+ is 1.85.

We do not measure and fit secondary interactions of outgoing

tracks. If such interactions occur close enough to the production vertex to cause a large error in the momentum determination for that track, it becomes less likely that an unambiguous fit will be obtained for the event, particularly for channels (b) and (d), which are of low constraint class already.

An estimate of the number of events lost for this reason is as follows: The greatest loss is for low momentum tracks having very large interaction cross sections, which more than counter balance their more easily determined momenta. π-p and p-p total cross sections are as large as 200 mb but the strange particle cross sections are much lower, comparable or less than 50 mb. If we need 10 cm. of track to determine a momentum adequately, the interaction probability $P_I = (1-e^{-\ell D\sigma_T})$, with ℓ=10cm. is .06 for σ_T=200 μb. We estimate that no more than 5% of the events are lost this way and there is no significant differential bias due to this depletion.

B. Interference in Pseudoscalar Meson Exchange

We will present the cross section computation for pion exchange. The K exchange case is identical.

The amplitude for pion exchange is the difference between two amplitudes appropriate to the diagrams in Fig. 18a which interchange the initial protons. The left-hand diagram gives

$$M_{12} = \frac{1}{(2\pi)^{3/2}} \frac{G}{(t-\mu^2)} \bar{\mu}_3 \gamma_5 \mu_1 A(M_{YK}, \cos\theta)$$

where A is the associated production amplitude at energy M_{YK} and center-of-mass angle θ. M_{21} is obtained similarly and $M = M_{12} - M_{21}$.

The differential cross section in the total c.m. frame is given by:

$$d\sigma = \frac{2\pi^2}{2\bar{P}\bar{E}} \frac{1}{4} \sum_{\text{spins}} |M|^2 \frac{d\bar{P}y}{2Ey} \frac{d\bar{P}k}{2Ek} \frac{d\bar{P}3}{2E3} \delta(W-Ey-Ek-E3) \times \delta^3(\bar{P}y + \bar{P}k + \bar{P}3) .$$

Using the fact that in the YK c.m.

$$\frac{d\sigma}{d\Omega}_{\pi p \to YK} = \frac{\pi^2}{4M_{YK}} \frac{P_f}{P_i} \sum_{\text{spins}} |A|^2$$

where P_i and P_f are the initial and final momenta, we obtain three terms. The $|M_{12}|^2$ term gives σ_A and the $|M_{21}|^2$ term σ_B which are related to one another by interchange of the initial protons. Thus

$$\sigma_A = \sigma(M_{YK}, t_1, \cos\theta, \phi)$$

$$\sigma_B = \sigma(M_{YK}, t_2, \cos\theta', \phi')$$

$t_1 = \Delta^2$, θ and ϕ are the variables defined in the text, and θ', ϕ' and t_2 are the comparable variables when one intercahnges the initial protons. σ_A and σ_B are included in the cross section formula (3) where we have removed the distinction between beam and target protons.

The term $2Re(M_{12}{}^*M_{21})$ gives rise to an interference cross section and can be computed exactly with knowledge of the associated production amplitude. Since data adequate for a meaningful phase shift analysis of associated production is not available we can only place limits on the size of this interference term.

We find easily that

$$\sigma_{int} = \frac{\sigma_A \sum_{spins} Re(M_{12}{}^* M_{21})}{\sum_{spins} |M_{12}|^2} + \frac{\sigma_B \sum_{spins} Re(M_{12}{}^* M_{21})}{\sum_{spins} |M_{21}|^2}$$

It can be shown[30] that in the approximation of small momentum transfer production

$$\frac{d^4\sigma_{int}}{dM_{YK}^2\, dt_1\, d\Omega} = \frac{-d^4\sigma(t_1+\mu^2)}{(t_2+\mu^2)} \frac{4m_p m'}{(t_2+(m_p-m')^2)} \left[R_1 + R_2 \cos\phi\right] \qquad \text{(A-1)}$$

where

$$R_1 = \frac{E'-\bar{E}}{m'm_p} Re(f_1{}^* f_2 - g_1{}^* g_2)$$

and

$$R_2 = \frac{\bar{p}p'}{m_p m'} Im(f_1{}^* g_2 \sin\theta + f_2{}^* g_1 \sin\theta')\sin\theta_p \quad .$$

Here E' and p' are the center-of-mass energy and momentum of the outgoing nucleon, θ_p is the c.m. production angle of this nucleon, where

$$t_1 = -m_p^2 - m'^2 + 2\bar{E}E' - 2\bar{p}p' \cos\theta_p ,$$

f and g are associated production amplitudes,

$$A = \frac{2}{\pi} \frac{M_{YK} p_i}{p_f} (f + g\vec{\sigma} \cdot \hat{p}_i \times \hat{p}_f) ,$$

so that

$$\frac{d\sigma}{d\Omega}_{\pi p \to YK} = |f|^2 + |g|^2 . \qquad (A\text{-}2)$$

We do not know f and g, however equation (A-2) permits us to set the limits

$$|R_1| \leq \frac{E'-\bar{E}}{m' m_p} \sqrt{\frac{d\sigma}{d\Omega} \frac{d\sigma}{d\Omega'}},$$

$$|R_2| \leq \frac{\bar{p}p'}{2 m_p m'} \sin\theta_p \sqrt{\frac{d\sigma}{d\Omega} \frac{d\sigma}{d\Omega'}}, \ (\sin\theta + \sin\theta')$$

We have used these inequalities to compute the limits on the interference cross section which we show in Figs. 15, 19, 20, and 23 as well as the maximum contribution to the $pp \to \Lambda p K^+$ total cross section, $\pm$ 8μb.

C. Numerical Computation of Meson Exchange Predictions

Given a function $F(X_1, X_2, --)$, it is a simple matter to numerically integrate it over any number of the variables X_i and thus produce distributions in any of the X_i as well as correlations between the variables implied by F. We use the Monte Carlo method to generate cross sections in the meson-exchange variables from the OPE formula (3). The technique involves generating a number of simulated events which have associated with them weights computed from (3). Weighted distributions of these events are the computed cross sections of interest and we then fit these histograms to produce the smooth curves displayed with the data.

The meson exchange cross-section prediction (3) is

$$d^4\sigma = F(M^2, \Delta^2, \theta, \phi)dM^2 d\Delta^2 d\Omega \quad .$$

We simulate events using this formula by using a random number generator to choose $\cos\theta$ between -1 and +1, ϕ between 0 and 2π and M^2, Δ^2 within the region of the Chew-Low plot. We can control the statistics in different parts of this region by picking either Δ^2 or M^2 first. If we choose Δ^2 first, then pick M^2 at random between the limits this value of Δ^2 implies and weight it by

$$M^2_{max}(\Delta^2) - M^2_{min}(\Delta^2) \ ,$$

we will have a higher density of points at small Δ^2, where the range of M^2 is small. The other order favors high M^2 and large Δ^2 where the range of Δ^2 is small. We have chosen the former method since pi exchange production of YK is peripheral and favors low YK mass.

Each event is then assigned an additional weight

$$W = F(M^2, \Delta^2, \theta, \phi)$$

and weighted distributions are computed precisely as the real data is plotted. In this way each of the selection criteria applied to the data can be included in predictions, in particular our systematic choice of the smaller momentum transfer, cuts on mass and Δ^2, etc. By constructing laboratory momenta we can include the procedures discussed in Appendix A for correcting scanning inefficiencies and thereby avoid the statistical difficulty involved in a maximum likelihood calculation with weighted events by including kinematic acceptance criteria in F.

Predictions obtained in this way and intended for display are fit with a Legendre expansion to P_7 to smooth statistical fluctuations.

REFERENCES

1. R. J. Oakes, Phys. Rev. 131, 2239 (1963).

2. B. Sechi-Zorn, R. A. Burnstein, T. B. Day, B. Kehoe, G. A. Snow, Phys. Rev. Letters 13, 282 (1964).

L. Piekenbrock and F. Oppenheimer, Phys. Rev. Letters 12, 625 (1964).

J. Schultz, R. Kinsey, W. Chinowsky, N. Rybicki, Bull. Am. Phys. Soc. Vol. 10, p. 529 (1965).

R. Engelmann, H. Filthuth, V. Hepp, E. Kluge, Phys. Rev. Letters 21, 587 (1966).

H. G. Dosch, R. Engelmann, H. Filthuth, V. Hepp, E. Kluge, Phys. Rev. Letters 21, 236 (1966).

R. A. Burnstein, Univ. of Maryland Tech. Report No. 469 (1965).

3. A. C. Melissinos, N. W. Reay, J. T. Reed, T. Yamanouchi, E. Sacharidis, S. J. Lindenbaum, S. Ozaki, L. C. L. Yuan, Phys. Rev. Letters 14, 604 (1965).

P. A. Piroue, Phys. Rev. Letters 11, 164 (1964).

W. J. Hogan, P. F. Kuny, A. Lemonick, P. A. Piroue, A. J. S. Smith, Bull. of the Am. Phys. Soc., Washington Meeting, p. 517 (1965).

W. A. Wenzel, private communication.

G. Alexander, O. Benary, B. Reuter, A. Shapiro, E. Simonpoulou, G. Yekutieli, Phys. Rev. Letters 15, 207 (1965).

4. R. Newman, W. Chinowsky, J. Schultz, W. B. Johnson, and R. R. Larsen, Phys. Rev. 158, 1310 (1967).

5. D. R. O. Morrison, CERN/TC/PHYSICS 66-20 (unpublished).

6. C. Dols, UCRL-8346, a quarterly report.

7. UCRL Engineering Note EET-1071. This method of beam control was suggested by J. Murray. The pulsing gear was constructed under the supervision of R. Force. We are indebted to them for the success of the operation.

8. We thank W. Wenzel for the use of equipment and aid in making this measurement.

9. W. E. Humphrey and A. H. Rosenfeld, Ann. Rev. Nucl. Sci. 13, 103 (1965).

10. F. T. Solmitz, A. D. Johnson, and T. B. Day, Alvarez Group programming note P-117 (unpublished).

11. UCRL 8030 (rev.) September 1967.

12. R. F. George, K. F. Riley, R. J. Tapper, D. V. Bugg, D. C. Salter, G. H. Stafford, Phys. Rev. Letters 15, 214 (1965).

13. A. R. Clyde (Ph.D. thesis) UCRL 16275.

14. Suppose the film contains N_0 events. Then the efficiency for scan A is $\epsilon_A = \frac{N_A + N_{AB}}{N_0}$, that for scan B is $\epsilon_B = \frac{N_B + N_{AB}}{N_0}$, and the combined efficiency is $\epsilon = \frac{N_A + N_B + N_{AB}}{N_0}$. If the scans are independent, $1 - \epsilon = (1 - \epsilon_A)(1 - \epsilon_B)$ and, therefore, $N_0 = \frac{(N_A + N_{AB})(N_B + N_{AB})}{N_{AB}}$. We can now solve for ϵ_A and ϵ_B and find the expressions given in the text.

15. E. Bierman, A. P. Colleraine, V. Nauenberg, Phys. Rev. 147, 922 (1966).

16. W. G. Holladay, Phys. Rev. 139B, 1348 (1965).

17. We take X = 350 MeV, the fitted result obtained by S. L. Glashow and A. H. Rosenfeld, Phys. Rev. Letters 10, 192 (1963).

18. J. E. Rush and W. G. Holladay, Phys. Rev. 148, 1444 (1966).

19. R. D. Tripp, D. W. G. Leith, A. Minten, R. Armenteros, M. Ferro-Luzzi, R. Levi-Setti, H. Filthuth, V. Hepp, E. Kluge, H. Schneider, P. Barloutaud, P. Granet, J. Meyer, and J. P. Porte, UCRL-17385 Rev. (to be published).

20. G. F. Chew and F. A. Low, Phys. Rev. 113, 1640 (1959).

21. E. Ferrari and F. Selleri, Suppl. Nuovo Cimento 24, 453 (1962).
J. D. Jackson and H. Pilkuhn, Nuovo Cimento 33, 906 (1964).
T. Yao, Phys. Rev. 125, 1048 (1962).

22. A. Dar and W. Tobocman, Phys. Rev. Letters 12, 511 (1964).
K. Gottfried and J. D. Jackson, Nuovo Cimento 34, 735 (1964).

23. J. K. Kim, Phys. Rev. Letters 19, 1079 (1967).

24. The meson exchange calculations use data from the following references for associated production and K^+p elastic scattering.

K^+p elastic scattering:

S. Goldhaber, W. Chinowsky, G. Goldhaber, Y. Lee, T. O'Halloran, T. F. Stubbs, G. M. Pjerrou, D. H. Stork, H. K. Ticho, Phys. Rev. Letters 9, 135 (1962).

T. F. Stubbs, H. Bradner, W. Chinowsky, G. Goldhaber, S. Goldhaber, W. Slater, D. H. Stork, H. K. Ticho, Phys. Rev. Letters 7, 188 (1961).

C. Wohl, private communication.

A. Bettini, M. Cresti, S. Limentani, L. Peruzzo, R. Santangelo, D. Locke, D. J. Crennel, W. T. Davies, P. B. Jones, Phys. Rev. Letters 16, 83 (1965).

W. Chinowsky, G. Goldhaber, S. Goldhaber, T. O'Halloran, B. Schwarzschild, Phys. Rev. 139B, 1411 (1965).

J. Debaisieux, F. Grard, J. Heughebaert, L. Pape, R. Windmolders, R. George, Y. Goldschmidt-Clermont, V. P. Henri, D. W. G. Leith, G. R. Lynch, F. Muller, J.-M. Perreau, G. Otter, P. Sällström, Nuovo Cimento 43A, 142 (1966).

W. De Baere, J. Debaisieux, P. Dufour, F. Grard, J. Heughebaert, L. Pape, P. Peeters, F. Verbeure, R. Windmolders, R. George, Y. Goldschmidt-Clermont, V. P. Henri, B. Jongejans, D. W. G. Leith, A. Moisseev, F. Muller, J.-M. Perreau, V. Yarba, Nuovo Cimento 45A, 885 (1966).

$\pi^-p \rightarrow \Sigma^+K^+$:

The data up to 1760 MeV/c is summarized by Holladay (Ref. 18).

D. Berley and N. Gelfand, Phys. Rev. 139, B1097 (1965).

D. R. O. Morrison, CERN/TCL Physics 66-20 (unpublished).

$\pi^- p \rightarrow \Lambda K^+$, $\Sigma^o K^o$, and $\Sigma^+ K^-$:

L. Bertanza, P. L. Connolly, B. B. Culwick, F. R. Eisler, T. Morris, R. Palmer, A. Prodell, N. P. Samios, Phys. Rev. Letters 8, 332 (1962).

Joseph Keren, Phys. Rev. 133, B457 (1964).

J. A. Anderson (Ph.D. thesis) UCRL-10838 (unpublished).

F. Eisler, R. Plano, A. Prodell, N. Samios, M. Schwartz, J. Steinberger, P. Bassi, V. Borelli, G. Puppi, G. Tanaka, P. Woloscjek, V. Zobolli, M. Conversi, P. Franzini, I. Mannelli, R. Santangelo, V. Silvestrini, Phys. Rev. 108, 1353 (1957).

O. I. Dahl, L. M. Hardy, R. I. Hess, J. Kirz, D. H. Miller, J. A. Schwartz, UCRL-17217 (submitted to the Physical Review).

25. a) W. J. Fickinger, E. Pickup, D. K. Robinson, and E. O. Salant, Phys. Rev. 125, 2082 (1962).

b) D. C. Rahm, R. R. Rau, A. M. Thorndike, and W. J. Willis, Phys. Rev. 123, 1465 (1961).

c) A. B. Wicklund, G. A. Smith, S. Wojcicki, W. Dunwoodie, and H. K. Ticho, UCRL-17791 (submitted to Phys. Rev. Letters).

d) G. Alexander, O. Benary, G. Czapek, B. Haber, N. Kidron, B. Reuter, A Shapira, E. Simopoulou, and G. Yekutieli, Phys. Rev. 154, 1284 (1967).

e) G. Alexander, A. Shapira, E. Simopoulou, and G. Yekutieli (preprint).

f) G. Ascoli, M. Firebaugh, E. L. Goldwasser, V. F. Kruse, R. D. Sard, COO-1195-75 (unpublished).

26. L. Stodolsky and J. J. Sakurai, Phys. Rev. Letters 11, 90 (1963).

27. G. Alexander, O. Benary, and U. Maor, (preprint, Weizmann Institute, August, 1967)

28. W. Rarita, R. J. Riddell, Jr., C. B. Chiu, and R. J. N. Phillips, UCRL-17523 (submitted to the Physical Review).

29. R. D. Newman (Ph.D. thesis) UCRL-17003 (1966).

30. B. Wicklund (private communication).